University of Tartu

Faculty of Science and Technology

Institute of Ecology and Earth Sciences

Department of Geography

Master thesis in Geoinformatics and Cartography

Synthetic Aperture Radar based flood mapping in the Alam-Pedja Nature Reserve in years 2005-2011

Martin Jüssi

Supervisors:

Kaupo Voormansik, PhD

Kārlis Zālīte, MSc

Tanel Tamm, MSc

Defence permitted:

Supervisor:

Head of Department:

Tartu 2015

Contents

Introduction

Flooding is a global environmental threat, causing large amounts of economic loss every year. According to Jongman, et al. (2014), annual economic casualties caused by floods may exceed $1 trillion by 2050. Recent changes in climate make flood mapping a valuable tool, as floods occur more often and cover larger areas than in previous decades (Kogan, et al., 2011). Remote sensing instruments provide a possibility to monitor wide-scale flood areas in regions where *in situ* measurements are often difficult to undertake. Optical remote sensing capabilities for flood monitoring are limited, as flooding often occurs during rainy seasons when clouds cover the ground. Synthetic aperture radar (SAR) provides a capability to monitor floods during virtually all weather conditions, and is therefore superior to optical systems (Townsend, 2002).

Due to its flat terrain and temperate climate, large areas in Estonia are subjects to floods several times every decade (Estonian Ministry of Environment, 2007). The flooding occurs mainly in large river drainage basins and affects mostly wetland and forested areas. The floods in Estonia have not been mapped in terms of remote sensing before, with the exception of Voormansik et al. (2014), where a detailed flood map of the drainage basin of river Emajõgi in central Estonia in April, 2010 was produced.

The objective of this study is to map annual floods in Alam-Pedja Nature Reserve in the period of 2005-2011 using SAR remote sensing imagery. The results of this thesis are based on data collected by ASAR, a remote sensing instrument on the European Space Agency's (ESA) Envisat satellite, which was operational from 2002 to 2012 (ESA, 2014a).

The strategy for algorithm selection for the flood area delineation was to provide a compromise between information reliability and rapidity of delivery, to analyse the possibility for rapid flood map production during critical flood events. Therefore, a supervised thresholding algorithm, used widely for flood mapping (e.g. Bates & De Roo, 2000; Townsend, 2002), was used in this study.

The paper is structured as follows. Section 1 gives an overview of flood monitoring needs and SAR capabilities, Section 2 describes the data and methods used for this study. In section 3, the results are presented. Section 4 discusses the results and challenges of the study, and in Section 5, conclusion of the study is provided.

1. Flood mapping

1.1. The need for flood mapping

Flooding is a major environmental threat that has caused wide-scale human and economic casualties around the world in the past years (Van der Sande, et al., 2003). Large-scale floods cause destruction of man-built infrastructures and limit access to natural resources (Kuenzer, et al., 2013). Documenting flood extents can inform communities about local flood risks to help property owners mitigate their economic losses, and direct governments into developing disaster mitigation measures and water management programs (Smith, 1994).

Additionally, boreal wetlands play an important role in the global carbon and water cycle, providing an important sink for atmospheric CO_2 (Griffis, et al., 2000). Global soil carbon represents 60% of total carbon on Earth, and approximately one third of the global soil carbon is stored in boreal wetlands. General atmospheric circulation models forecast the increase in temperature and decrease in soil moisture in high latitudes, which will accelerate the decomposition of organic material and the flow of CO_2 to the atmosphere (Griffis, et al., 2000). Furthermore, floodplains provide habitat and breeding environment for fish and other aquatic species (Kuenzer, et al., 2013). Therefore, providing periodical overview of wetlands remains important for conservation of the environment.

Large-scale flood areas are very difficult to map using *in situ* observations, and due to time-constraints in emergency situations, fast acquisition of information is needed (Martinis, et al., 2009). Increasing flood mapping capabilities can be offered by satellite remote sensing instruments, which provide a large-scale, near-real time overview of geographical regions. Satellite-based flood maps can be used effectively for disaster prediction and mitigation, water management and environmental awareness (Smith, 1997).

1.2. Floods and flood mapping in Estonia

Estonia is subject to floods several times a decade. There are two types of regions in Estonia which are at significant risk of flooding: coastal areas where the risks are associated with rising water levels in rivers, lakes or the sea, and mainland areas where extensive amount of water produced by rapid snowmelt or heavy rains gets trapped around rivers and reservoirs (Estonian Ministry of Environment, 2007).

Flood situations in the risk areas need to be recorded and mapped, as they might endanger the people, their property and economy. According to the Estonian Ministry of Environment (2007), in January

2005, a storm in Estonia caused damage worth over 47 million euros, of which a large amount was caused by floods. To minimize the damage to the economy and environment in the future, the European Parliament and European Council developed a flood risk assessment and management directive (2007/60/EC) in October 2007. The directive states that flooding in each risk area needs to be assessed and the flood areas mapped (Estonian Ministry of Environment, 2007).

In 2011, the Estonian Ministry of Environment pointed out 20 highly populated areas in Estonia that are at significant risk of flooding. For each area, potential flood extents were modelled using the Digital Elevation Model (DEM), provided by Estonian Land Board (Estonian Ministry of Environment, 2013).

However, previous studies (e.g. Nardi, et al., 2013) show that actual floods may differ from the DEM-based models. This is likely due to the fact that the water level rises and lowers very fast during the springtime floods, and can be affected by melting snow, precipitation, wind, porosity of the surface and other factors.

1.3. Flood monitoring with SAR

1.3.1. SAR overview

SAR is an active microwave remote sensing instrument, which can provide high-resolution images of the Earth's surface during both day and night and virtually under all weather conditions (Hess, et al., 1990; Wang, et al., 1995). The sensor's ability to penetrate cloud cover and detect water under forest canopy makes an airborne or satellite SAR system a powerful tool for flood monitoring, as floods often associate with heavy rain, and suffuse forested areas around rivers and wetlands, where it is almost impossible for optical remote sensing instruments to image the water (Townsend, 2002). Although flood and wetland mapping with optical remote sensing has also been very common (e.g. Johnston & Barson, 1990; Enslin & Sullivan, 1974), SAR systems are superior to optical systems due to the aspects mentioned above. The first algorithms for flood detection with SAR were introduced in the early 1980s (e.g. Lowry, et al., 1981) and have been developed further ever since. Nowadays SAR systems are widely used for flood mapping (Martinez & Toan, 2007), and prove especially useful in small- to medium-sized drainage basins where inundation often recedes before meteorological conditions improve (Schumann, et al., 2007; Martinis, 2010).

1.3.2. Polarization of SAR signal

The polarization of a SAR instrument refers to the orientation of the transmitted SAR beam's electric field vector. In case of the vector oscillating in the horizontal direction, the beam is said to be "H" polarized. In case of oscillation perpendicular to the horizontal direction, the beam is known as "V"

polarized. Polarization is measured for both transmitted and received SAR signal, giving it four possible combinations (HH, VV, HV, VH) (Centre for Remote Imaging, Sensing & Processing, 2001).

SAR polarization is a key factor in flood detection. It is proven in several previous studies (e.g. Baghdadi, et al., 2001; Henry, et al., 2006) that HH-polarized images are considered more adequate for flood detection than VV- or cross-polarized images. This is mostly due to the fact that HH-polarization gives the highest distinction in backscatter values between dry and wet forested areas. However, combining different polarizations can lead to improved flood maps, as HV polarization is less sensitive to surface conditions, especially wind-induced roughness (Henry, et al., 2006).

Although Envisat ASAR, the instrument used for this study, produced data in several polarization configurations (including HH, VV, HH/HV, VV/VH), only HH-polarized images were used in this study due to no availability of other data in the focus period.

1.3.3. Open Water

Many flood mapping SAR algorithms model open water as a perfect smooth surface which reflects most radiance away from side-looking SAR sensors (Figure 1). This generates virtually zero backscatter, making open water appear dark on a SAR image (Sarti, et al., 2001; Horritt, et al., 2003). Such areas can be detected due to the contrast with the surrounding rougher areas which generate more backscatter and therefore appear brighter on the images (Martinis, et al., 2009).

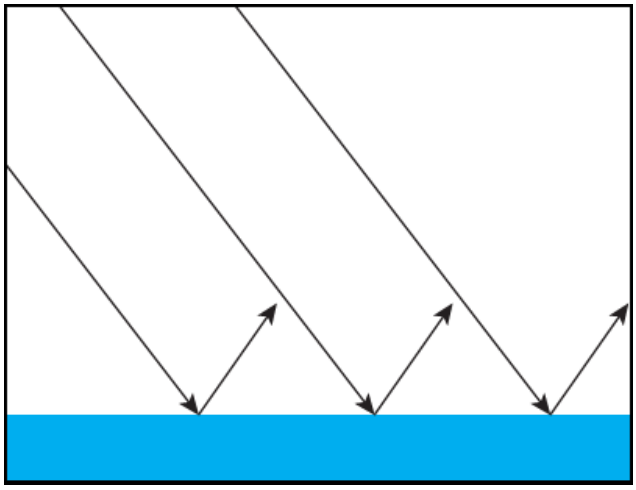

Figure 1. SAR signal scattering mechanism from a perfectly smooth water surface.

According to Drake & Shuchman (1974), short wavelengths show a higher contrast ratio between land and water than longer wavelengths, as the electromagnetic radiation only interacts with objects same or larger than its wavelength. Therefore, the longer the wavelength, the smaller the number of possible rough features on land that cause backscatter. Therefore, smooth land surfaces appear dark and similar to water on longer wavelength images. Consequently, shorter wavelength SAR images appear to be

more suitable for open water detection purposes than those of longer wavelength. Envisat ASAR provides images in C-band, with wavelength of 5.6 cm. C-band SAR systems are widely used for environmental monitoring, and are proven to distinguish dry land from open water (Canada Centre for Remote Sensing, 2015).

1.3.4. Flooded vegetation

To model the radar backscatter from wetland ecosystems, it is necessary to note that each vegetation layer affects the radar signature. According to Kasische & Bourgeau-Chavez (1997), a forested area can be divided into three layers (Figure 2): a canopy layer which consists of small branches and foliage, a trunk layer consisting of large trunks and branches, and a ground layer, which, in the case of flood, may be covered by water.

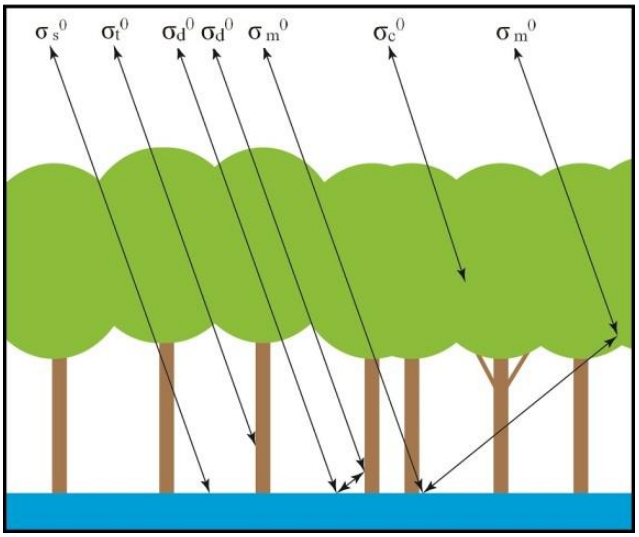

Figure 2. SAR signal backscatter mechanism from a flooded forest

Floods under forest canopy can be detected by a strong rise in backscatter values when compared to the backscattering from the same forested areas in dry conditions (Zalite, et al., 2013). This is due to the reflection of the radar pulse from the horizontal water surface and backscattering from the trunks and branches of the vegetation, resulting in strong signal return. Diffuse scattering from the ground during dry conditions reduces the corner reflection effect of the pulse, resulting in less signal return and darker image tones (Hess, et al., 1990). The backscatter mechanism from a flooded forested area, as shown in Figure 2, can be described with an equation:

$$\sigma^0 = \sigma_c^0 + \alpha_c^2(\sigma_m^0 + \sigma_t^0 + \sigma_s^0 + \sigma_d^0) \quad (1)$$

The total microwave backscatter (σ^0) consists of backscattered radiation from the canopy (σ_c^0), tree trunks (σ_t^0), surface (σ_s^0), double bounce from the trunks and surface (σ_d^0), and other multipath backscattering (σ_m^0). According to Townsend (2002), the highest influence on the total backscatter from flooded forest areas is given by the water-trunk reflection (σ_d^0); the difference between

backscatter coefficients obtained from flooded and non-flooded conditions under forest canopy can be up to 10 dB.

The canopy and trunk attenuation coefficient (α_c) is a function of radar frequency, derived from the transmissivity of the crown and trunk layers of the forest. Higher frequencies, for example in X-band SAR, refer to higher interference with foliage and canopy than lower frequencies in P- or L-band SAR, which results in loss of canopy penetration ability for higher frequency instruments. Therefore, lower frequencies like in L-band are generally preferred for forest flood mapping (Kasische, et al., 1997). However, due to the fact that SAR image resolution is directly proportional to bandwidth (Voormansik, et al., 2014), higher resolution imaging is possible in shorter wavelength bands like in X- or C-band, than in L-band. C-band can provide a compromise between spatial resolution and canopy penetration for flood mapping.

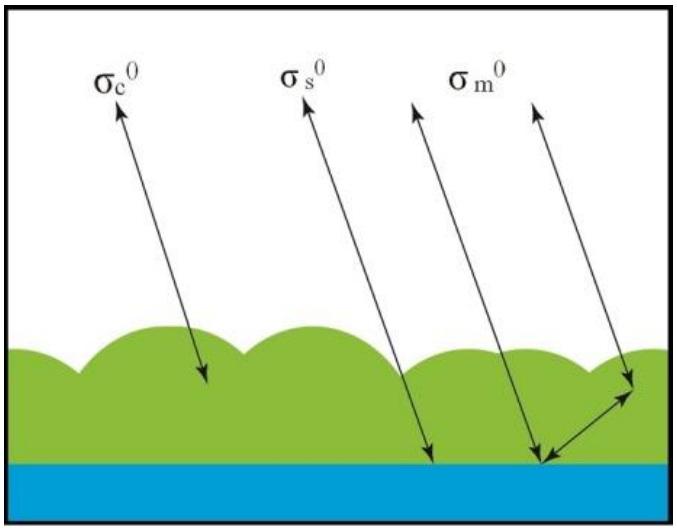

Figure 3. SAR signal backscatter mechanism from a flooded non-woody shrub area

According to Kasische & Bourgeau-Chavez (1997), flooded non-woody shrub areas can be modelled similarly to flooded forested areas, by eliminating all items on the trunk layer (Figure 3). This leads to a simplified equation:

$$\sigma^0 = \sigma_c^0 + t_c^2(\sigma_m^0 + \sigma_s^0) \quad (2)$$

Here the elements pertaining to the trunk layer are removed. The transmission coefficient (t_c^2) refers to the transmissivity of the vegetation canopy layer.

1.4. Challenges in flood monitoring

Although the weather conditions generally do not affect the ability for SAR to image the Earth, the presence of heavy rain might affect the accuracy of flood monitoring. Strong wind or heavy rain can cause roughening of the water surface, resulting in rise of backscatter close to the levels of surrounding

dry land or higher. This is most significant in transient areas between the flooded and non-flooded zones, where the radar backscatter increases gradually, complicating the accurate delineation of flooded areas. In addition, emergent vegetation or buildings in open flooded areas lead to the increase of backscatter due to multiple reflections, reducing the accuracy of SAR-based flood maps (Mason, et al., 2010).

Also, it is noted in previous studies (e.g. Koskinen, et al., 1997) that wet snow in open areas causes very low backscatter to a C-band SAR, and is therefore difficult to distinguish from open water. In the study of Voormansik et al. (2014), it was noted that rough wet fields might produce very high backscatter in X-band SAR images, which makes it difficult to distinguish them from flooded forests. Due to these effects, weather conditions before and during the image acquisitions need to be known, or image interpretation may be prone to misclassification.

The significance of errors resulting from these challenges depends on the methodology used for flood delineation. For the split-based thresholding method used in this study, the significance of errors in classification depends on the level of information about weather conditions during the acquisition and precision of the manual delineation by the interpreter. The importance of manual (supervised) thresholding is confirmed by the study of Matgen, et al. (2011), which states that the accuracy of contemporary SAR-based flood detection algorithms is dependent on the operator's subjective impression and fine-tuning of the algorithms, with fully automatic processes still being very rare. A recent example of automatic flood detection is the study of Martinis et al. (2014), where a fully automated TerraSAR-X based flood mapping service is presented.

The flood detection mechanisms for open and forested areas, mentioned earlier in this section, were used as a base for understanding the flood extraction techniques from radar images. For identifying the potential reasons for the presence of water in the radar images, weather data was obtained for each of the acquisition dates. Geo-referenced photos, taken in the study area during the acquisition of April 18, 2010, were used for improving the accuracy of image classification. More elaboration on the methodology used in this study is provided in Section 2, and problems encountered are discussed in Section 4.

2. Input Data and Flood Map Generation

2.1. Data

2.1.1. Study Area

The Alam-Pedja Nature Reserve is situated in the central part of Estonia, north-east of Lake Võrtsjärv. It covers an area of 347 km^2, and being one of the wettest areas in Estonia, is subject to floods several times each decade. The floods in Alam-Pedja occur most often in spring, but in some years the water levels have been the highest in December or January. Mires occupy about half of the total area of the nature reserve, and rivers Emajõgi, Põltsamaa and Pedja join in the area. The rivers and mires are surrounded by deciduous, coniferous and mixed temperate forests. The deciduous forests consist mainly of birches, while coniferous forests include mostly spruces and pines. In the surroundings of the nature reserve the ground is more elevated and agricultural lands on automorphic soils are found. Due to the low population density in the Alam-Pedja Nature Reserve, flooding is not a serious threat to the local inhabitants or economy (Aaviksoo, et al., 2000).

The selected study area is shown in Figure 4. For this study, flood extent values were calculated for the area within the borders of the Alam-Pedja Nature Reserve, and additionally for a larger area around the reserve (black rectangle in Figure 4), to give an overview of the whole floodplain in the region. The total area measured is 1 683 km^2, spanning 33 km from north to south and 51 km from east to west.

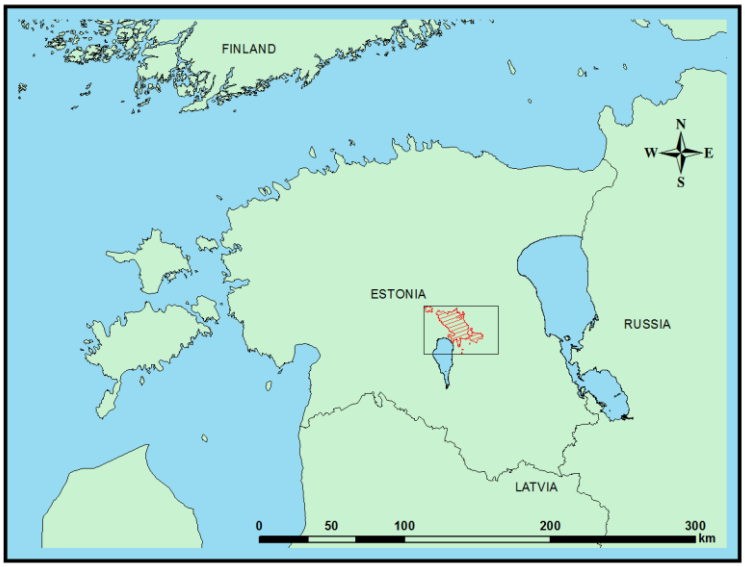

Figure 4. Location of the Alam-Pedja Nature Reserve (marked in red) with the additional study area shown around it with the black rectangle.

2.1.2. Water level data

Water level data used in this study was obtained from three hydrology survey stations around the Alam-Pedja Nature Reserve – Tartu-Kvissentali, Tõrve and Pajusi, situated on rivers Emajõgi, Pedja and Põltsamaa, respectively (Figure 5). The stations are operated by the Estonian Weather Service (EWS). Water level data for each day in years 2005-2011 (Figure 6) was provided by EWS, and processed to find the maximum water levels in the focus period. A water level rise was of interest for this research when the water levels in Tartu-Kvissentali, Tõrve and Pajusi stations were over 200, 150 and 100 cm over the local long-time zero, respectively. This happened in a total of 71 days in the focus period, in January 2005, December 2008, April 2009, April 2010 and April 2011, with an average of 14 days of flood per year. According to EWS, the water level in April 16, 2010 had the third highest value (330.3 cm over a local long-time minimum) in the measurement history in Tartu since year 1942 (EWS, 2014).

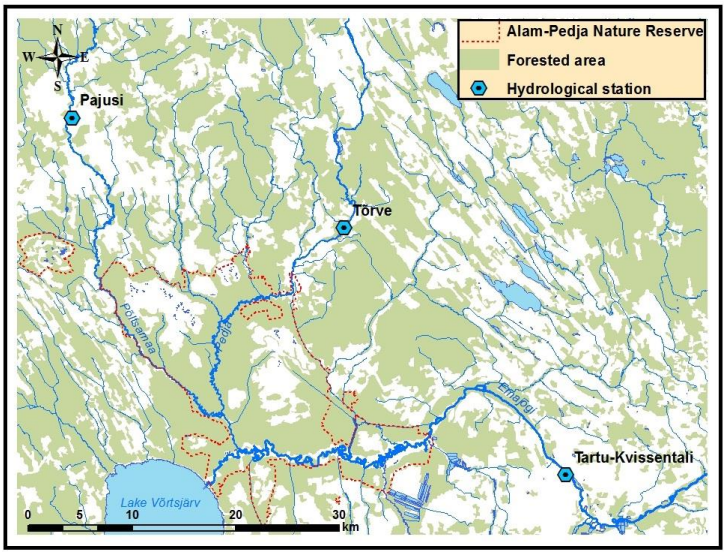

Figure 5. Tartu-Kvissentali, Tõrve and Pajusi hydrological stations

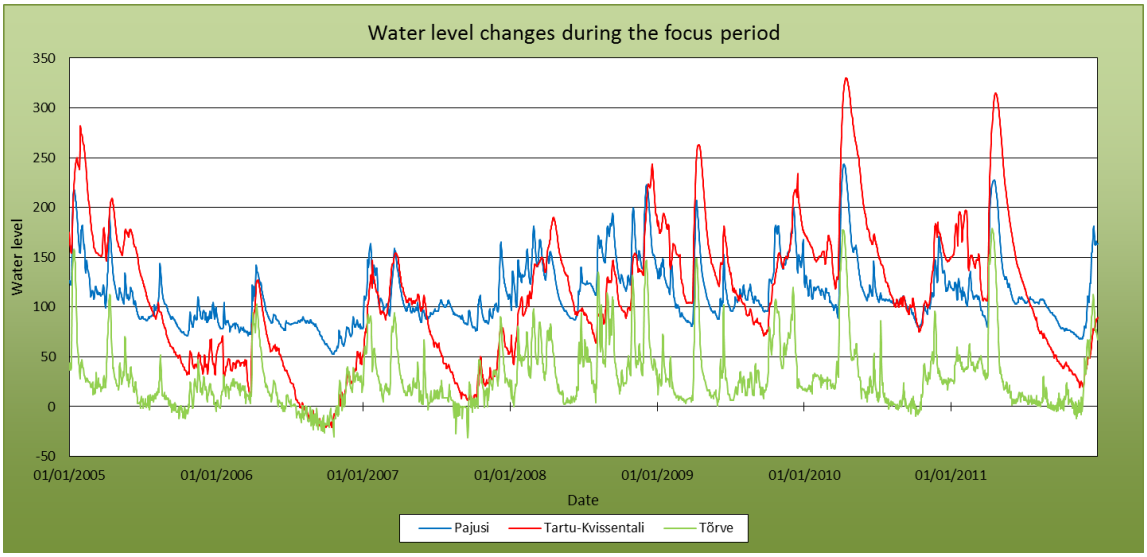

Figure 6. Water levels (cm) measured in the EWS hydrological stations through the years 2005-2011.

2.1.3. SAR data

For this study, Envisat ASAR images were ordered from the ESA. During the flood periods in 2005-2011, 24 HH-polarized Envisat ASAR images were available. The images acquired were C-band (5.6 cm wavelength), with pixel spacing of 75 m and spatial resolution of 150 m. The incidence angle of the images in the study area varied between 22.3° (April 21, 2011) and 41° (April 24, 2010). The acquisition dates along with details of the SAR images are shown in Table 1. Within the periods mentioned in the previous section, the floods were mapped on dates when the water level of the river Emajõgi was closest to the maximum and HH-polarized ASAR images were available. Due to the lack of Envisat coverage in December 2008, the flood in that year was not mapped in this study.

Table 1. Parameters of the Envisat ASAR images used in this study, along with weather conditions and water levels during the acquisitions.

Acquisition date	Incidence angle (degrees, left to right)	Track	Temperature (Celsius)	Total precipitation 1 hour before (mm)	Total precipitation 24 hours before (mm)	Water level in River Emajõgi	Water level in River Põltsamaa	Water level in River Pedja
12.01.2005	33.5-36	ASCENDING	5.7	0	0.6	217	217	158
21.01.2005	31.0-28.4	DESCENDING	-1.1	0	0	249	64	189
08.12.2009	36-33.5	DESCENDING	0.3	n/a	n/a	216	190	90
15.12.2009	25.42-28.28	ASCENDING	-15.5	n/a	n/a	221	138	19
14.04.2010	28.4-25.75	DESCENDING	10.7	0	0	330	239	158
18.04.2010	28.12-30.86	ASCENDING	7.8	0	1.6	329	222	130
24.04.2010	38-41	ASCENDING	2.4	0	1.2	315	191	84
15.04.2011	37.0-34.6	DESCENDING	6.8	0	0	295	226	176
21.04.2011	22.3-25.7	ASCENDING	10.4	0	0.2	315	224	143

2.1.4. Weather conditions

The closest weather station to the study area was the EWS Tartu-Tõravere station, located in 58°15'52.92" of latitude and 26°27'42.12" of longitude, 29 km SE from the centre of the Alam-Pedja Nature Reserve. The precipitation, water level and temperature conditions in prior to the acquisition of images are also shown in Table 1. No precipitation information was available around the image acquisitions in December 2009. Weather conditions during the acquisitions were generally relatively dry, with a small amount of precipitation occurring in January 12, 2005, April 18 and 24, 2010, and April 21, 2011 (EWS, 2014).

2.1.5. Reference data

For the study of Voormansik et al. (2014), a ground observation campaign had been carried out in the Emajõgi drainage basin in March-April, 2010. As the study area of Voormansik et al. covers also the Alam-Pedja Nature Reserve and the region around it, the results of the campaign could also be used as reference data for this study. The spring flood in 2010 was documented on photos during the ground observation campaign through March and April. For this study, *in situ* photos taken in April 17-18, 2010 in 40 locations around the flood were used (red dots in Figure 7). An example photo is seen in Figure 8. Regarding these photos, training areas were drawn on the April 18, 2010 flood image, shaped according to features visible on the photos. Additional orthophotos, provided by the Estonian Land Board, were analysed together with *in situ* photos for providing better understanding of the landscape around the locations.

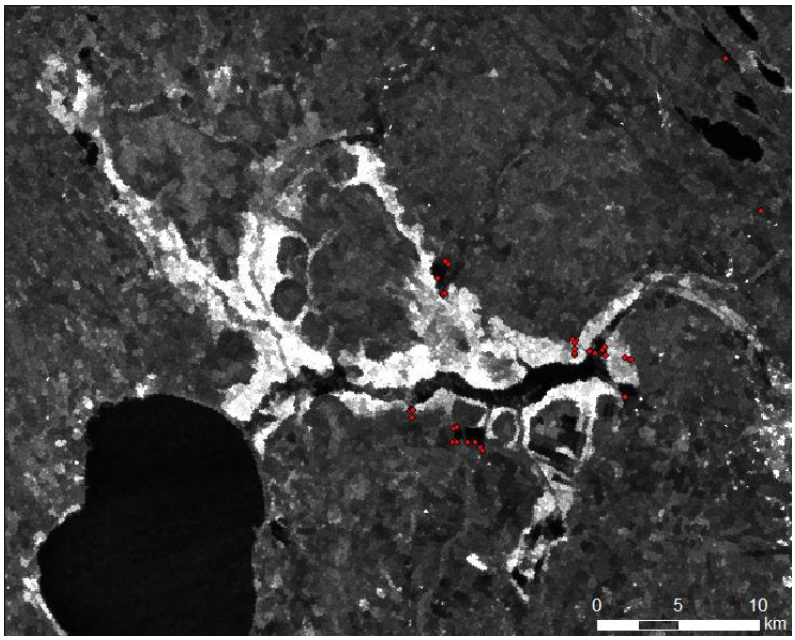

Figure 7. Locations of the reference images taken in April 17-18, 2010, shown on the April 18, 2010 ASAR image. Each red dot represents one location where a 360 degree view was documented.

Figure 8. Picture of a flooded field in Laeva, taken on April 18, 2010 (Voormansik, et al., 2014).

2.2. Methods

2.2.1. SAR image processing in NEST

The images were processed using Next ESA SAR Toolbox (NEST) version 4.1, software developed by Array Inc. especially for SAR image processing (ESA, 2014b). To enhance the usefulness of the SAR images, a despeckling procedure was performed on each image. Speckle, a signal-dependent noise, is natural to any images obtained by coherent radiation, including SAR images. It reduces the readability and decreases the usefulness of the images for both human and automatic interpretation (Mascarenhas, 1997).

The acquired Envisat ASAR images were despeckled using a Refined Lee filter, a widely used local area statistic filter which eliminates the speckle while preserving the edges, linear features, point targets and texture information (Lee, et al., 1994).

Each SAR image was calibrated to a linear scale, and using a simple equation shown below (3), the pixel values were re-calculated to match the scale of the April 18, 2010 ASAR image, which was referenced with photos. This was done to remove differences in backscatter values caused by incidence angle and therefore make it possible to use the same threshold value levels on each image.

$$Y = \alpha X + \beta \tag{3}$$

In the equation (3), X represents the total set of pixel values in the image processed. X is multiplied by a coefficient α which scales the set of values to match the set of the referenced April 18, 2010 image. β is the free variable, added for shifting the lowest value to the same level with the referenced image, and Y is the new set of pixel values. The values of α and β were obtained by observing the differences in the minimum and maximum values in the pixel sets, and are shown in Table 2.

Table 2. α and β values for each image.

Acquisition date	12.01.2005	21.01.2005	08.12.2009	15.12.2009	14.04.2010	18.04.2010	24.04.2010	15.04.2011	21.04.2011
Coefficient (α)	0.9908	1.7676	1.6652	2.1112	0.8397	1	1.9005	1.4476	0.8217
Free variable (β)	-0.0028	0.0040	0.0019	0.0075	0.0023	0	0.0059	0.0025	-0.0003

Floods on the SAR images were detected using a manual split-based image thresholding method, used widely for flood mapping (e.g. Bates & De Roo, 2000). As noted in previous chapters, water in open areas generates virtually no backscatter and appears very dark on SAR images, giving high contrast with surrounding forested areas, especially flooded forests, which appear very bright due to double-bounce scattering. As mentioned earlier in Section 2.1.5, training areas with open water, flooded forested and non-flooded regions were selected from the ASAR image of April 18, 2010 (Figure 9).

Regarding the data tables, histograms were produced and the flood/non-flood threshold was established between two peaks (Figure 10). The threshold was established manually so that the sum of falsely classified pixels remained minimal. The size of training areas in pixels and the error percentage in classification due to value overlap are given in Table 3.

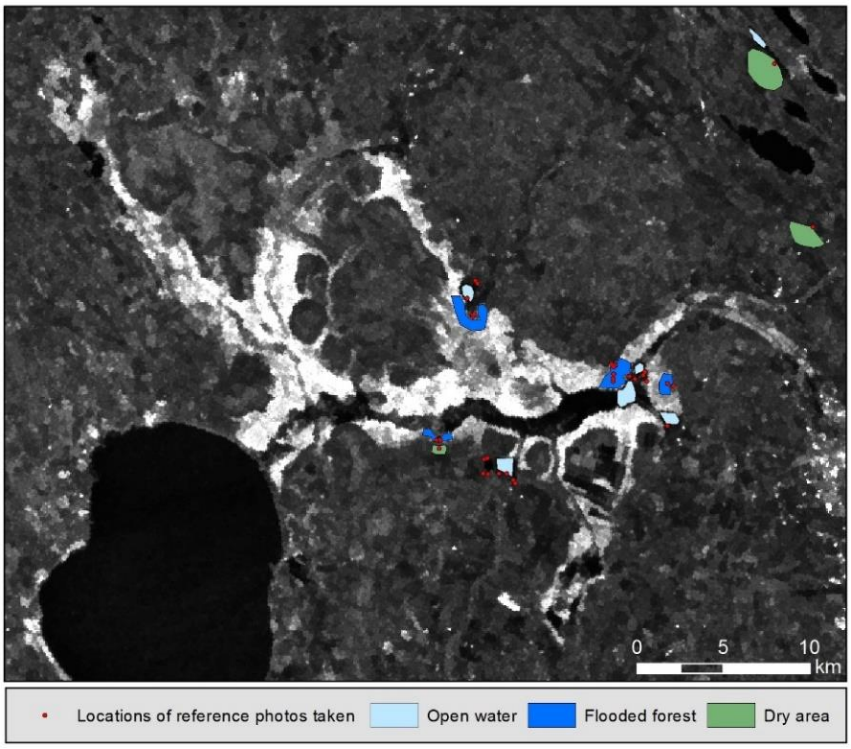

Figure 9. Training areas on the ASAR image of April 18, 2010.

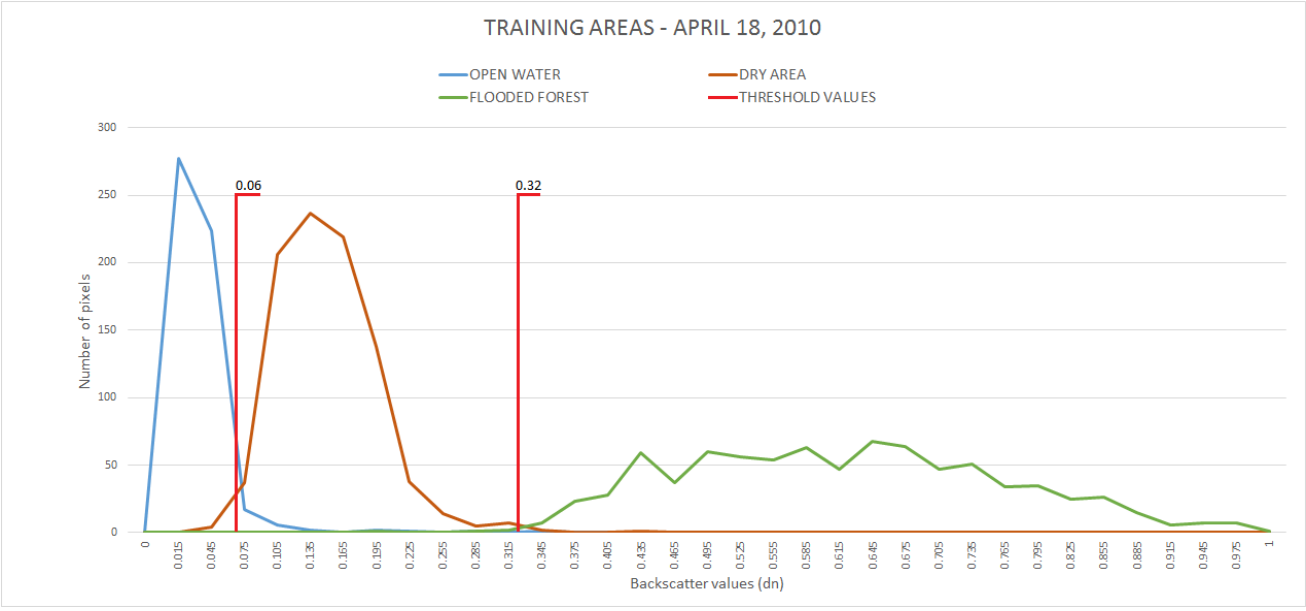

Figure 10. Histograms showing backscatter values of the training areas, with threshold values between flooded open areas/dry areas and dry areas/flooded forested areas.

Table 3. Number of pixels and error estimates of training areas on the April 18, 2010 ASAR image.

	Total number of pixels	Falsely classified pixels	% of false/all
Open flood	531	30	5.65
Dry area	908	7	0.77
Flooded forest	824	4	0.49

The images were then converted to Boolean images, using the NEST tool "Create Band from Math Expression" with pixels fallen within the "flooded" range having the value of 1 and "non-flooded" pixels 0. For creating contiguous areas, the images were smoothed using a 3 x 3 pixel median filter which removed small isolated pixels with values significantly higher or lower than their adjacent pixels. Finally, the images were reprojected to the L-EST'97 coordinate system, and stored in GeoTIFF format for easier interoperability between different software.

2.2.2. Raster processing and vectorization in ArcMap

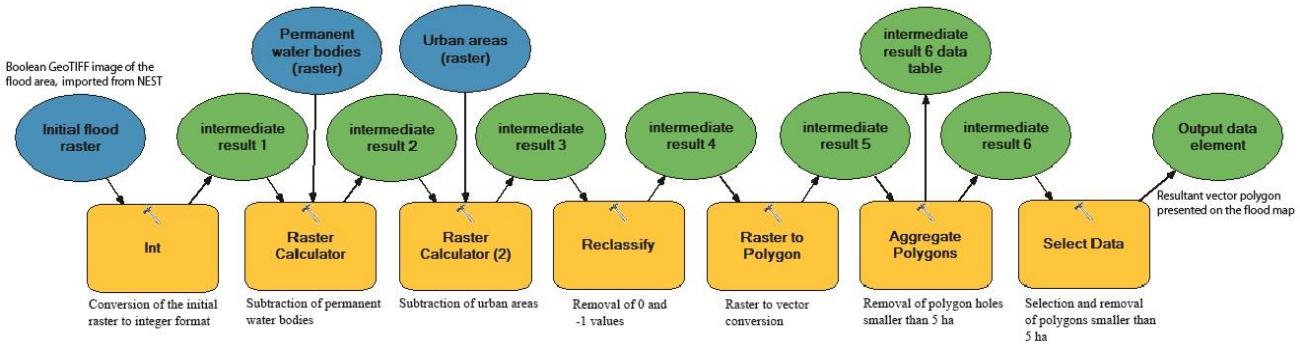

Figure 11. ArcGIS model developed for conversion of the ASAR-based Boolean images to vector data. Input data are shown in blue ovals, processing steps in yellow boxes, and results (including intermediate results) in green ovals.

The GeoTIFF images were imported to ESRI ArcMap 10.2 software for further processing. Using Corine 2006 land cover data (European Environment Agency, 2006) and additional vector data provided by Regio Ltd., masks containing permanent water bodies, urban areas and forests were created. An ArcGIS Model Builder model, shown in Figure 11, was developed for automatic processing and vectorization in ArcMap. The GeoTIFF images imported from NEST were converted to integer format, for easier processing in ArcMap. Mask layers representing permanent water bodies and urban areas were subtracted from the flood areas, and the remaining pixels were vectorized, using the ArcGIS "Raster to Polygon" tool. The polygon edges were simplified to prevent pixelation in final images. Due to relatively coarse spatial resolution, polygons and polygon holes smaller than 5 ha were considered as noise and removed, using ArcMap's functions "Aggregate Polygons" and "Select Data by Attributes".

The resulting polygons were considered as flooded areas in this study, and flood maps were composed. Each flood map is presented and described in the next section.

Backscatter values on additional pixels were characterised on the April 18, 2010 ASAR image to test the accuracy of the classification on the training areas. Regarding the pixel values within the test areas, an error matrix, introduced by Congalton (1991), was generated to assess the accuracy of classification. Test areas were generated for dry, open water and flooded forested areas (Figure 12), derived from photos described earlier in Section 2.1.5. Matching value pixels in both the flood map and the test areas were measured against total amount of pixels on the test areas, and a percentage of misclassification was calculated. The accuracy measurement in this study was based on a total of 396 pixels within and around the flood area, which constituted 1% of the total flood area in April 18, 2010. The results of the error measurement are also discussed in the next section.

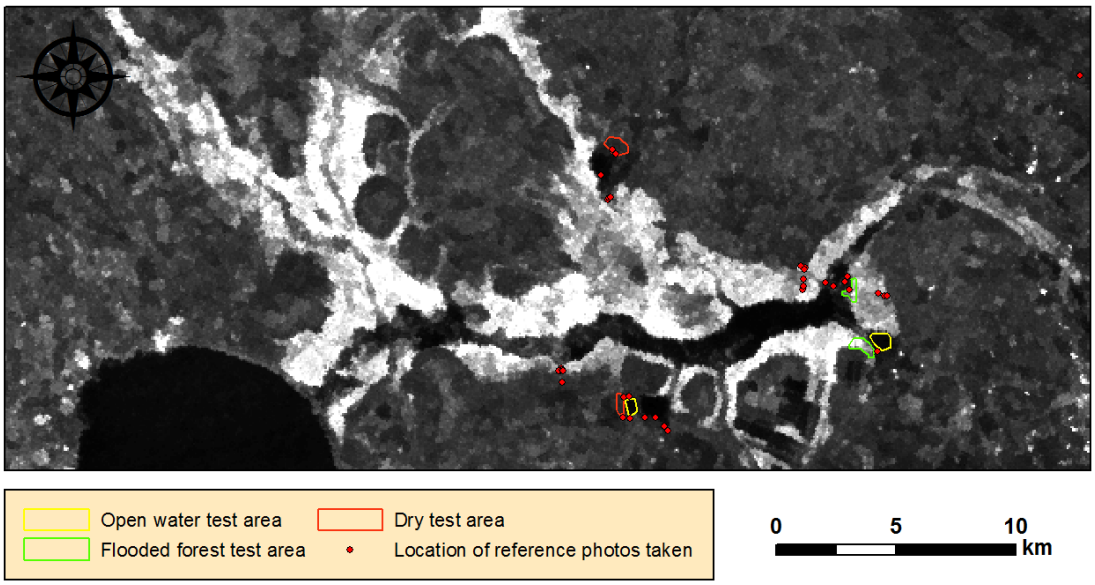

Figure 12. Test areas selected for assessing the accuracy of image classification.

3. Results

The results of this thesis, the SAR-derived Alam-Pedja flood map images, are shown and discussed below.

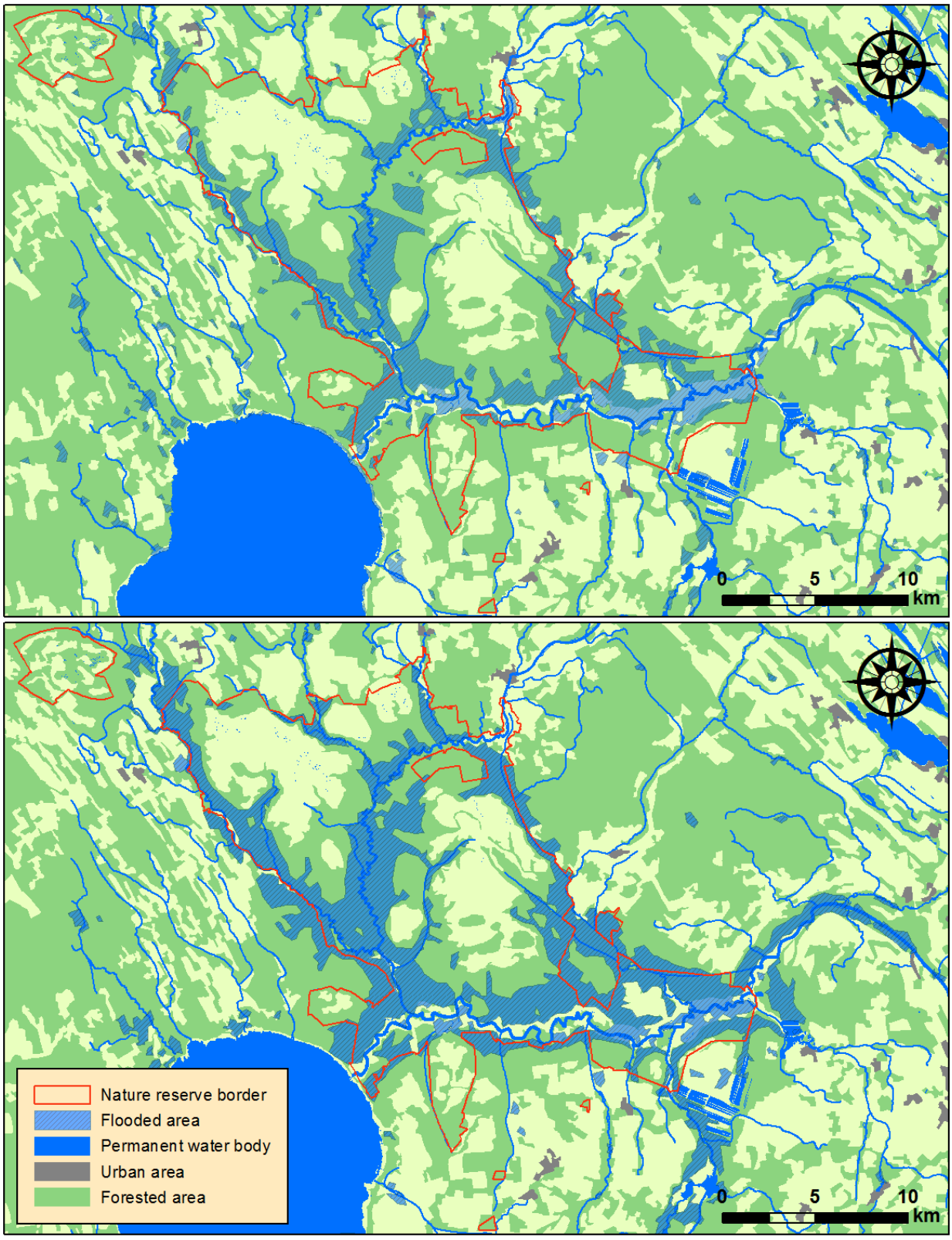

Figure 13. Flood maps of January 12 (above) and January 21 (below), 2005.

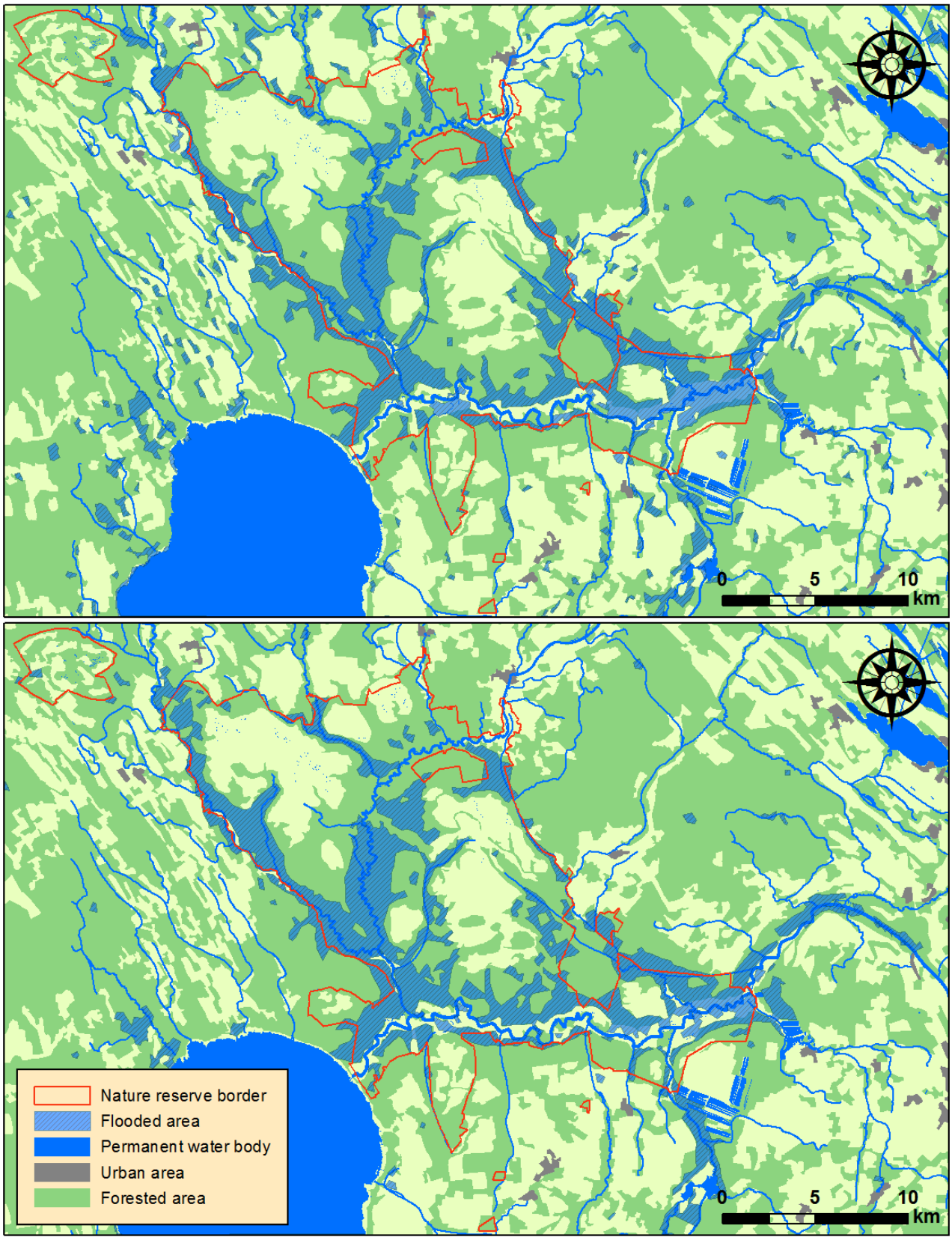

Figure 14. Flood of December 8 (above) and December 15 (below), 2009.

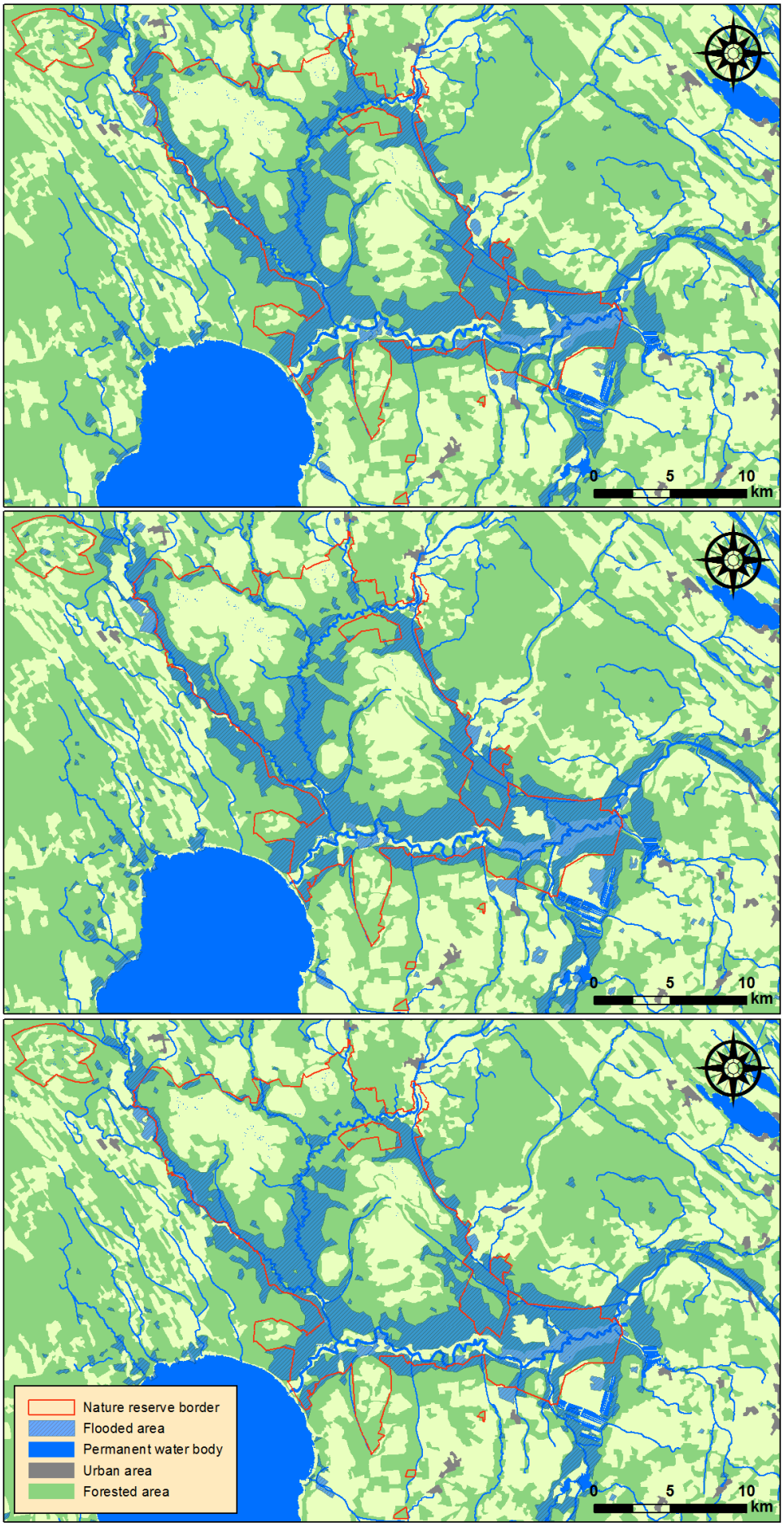

Figure 15. The flood maps of April 14 (top), April 18 (center), and April 24 (bottom), 2010.

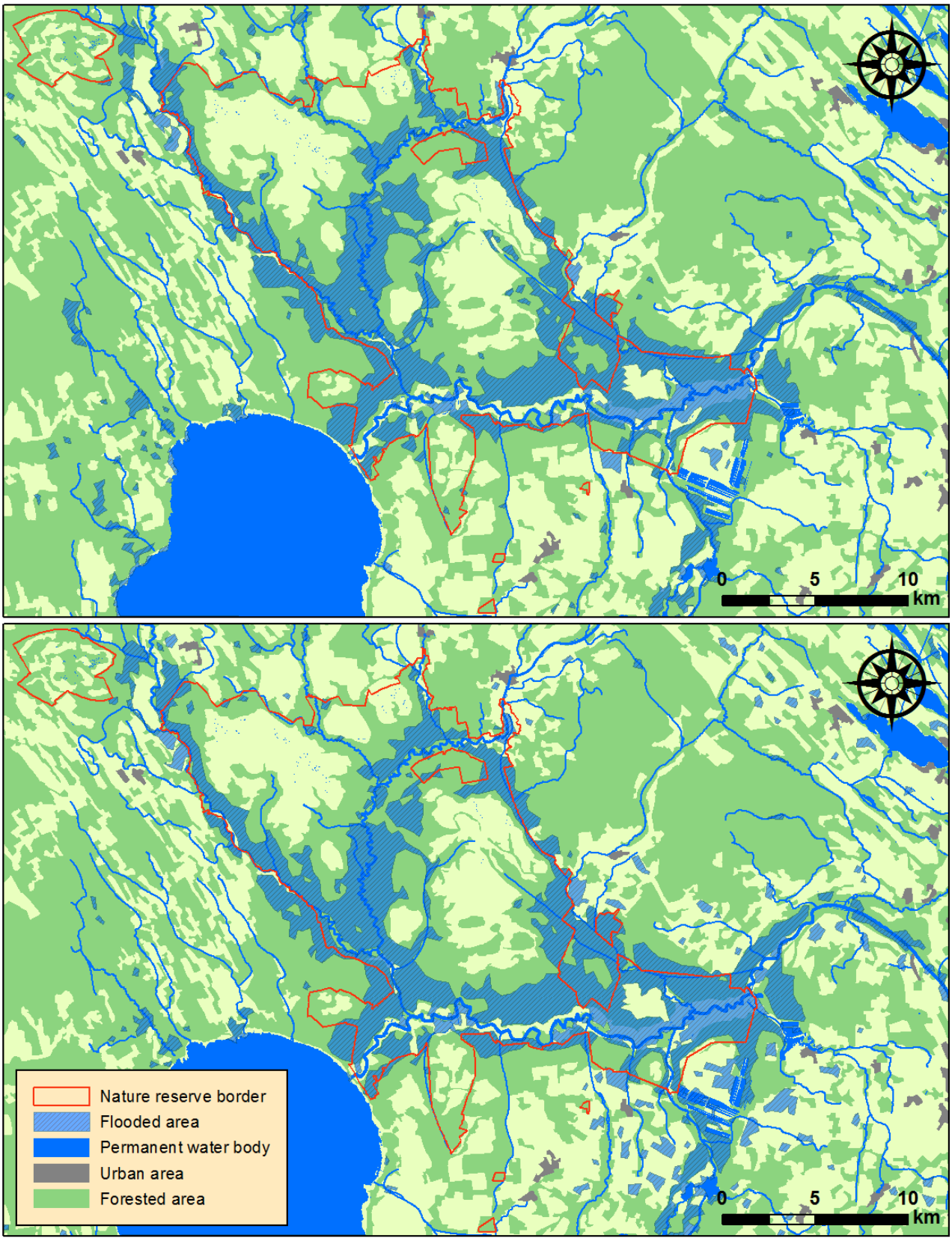

Figure 16. Flood maps of April 15 (above) and April 21 (below), 2011.

The flood of January 2005 is shown in Figure 13. The Alam-Pedja flood area on January 12 accounted for 103 km^2, and by January 21, it had swollen to 166 km^2. It can be seen that the total flood area in the study area also increases, from 124 to 188 km^2.

Figure 14 shows the flood maps from December, 2009. The recorded flood area within the Alam-Pedja Nature Reserve was 116 km^2 on December 8 and 129 km^2 on December 15. The total flood area within the study area was 152 km^2 on December 8, and had shrivelled to 145 km^2 by December 15. The difference in water dynamics inside and around the nature reserve could be explained by the flow of water from surrounding fields into the lower-elevated nature reserve.

By December 15, 2009, water level in the river Emajõgi (221 cm) had risen when compared to that in December 8 (216 cm), and in the rivers Pedja and Põltsamaa, the water levels dropped. This can be seen when comparing the maps, with broader areas around the river Emajõgi being flooded on December 15.

The flood areas of April 2010 are shown in Figure 15. The Alam-Pedja flood area was 175 km^2 in April 14, 180 km^2 in April 18 and 169 km^2 in April 24. The flood dynamics differ slightly from the water level dynamics in 2010. This could be due to precipitation, which was also recorded on April 18 and 24. The total flood area in the study region was 205 km^2 in April 14, 212 km^2 in April 18, and 196 km^2 in April 24.

The flood areas of April 2011 are shown in Figure 16. The extent of the Alam-Pedja flood was 156 km^2 in April 15, and 178 km^2 in April 21. The total flood area in the study region was 189 km^2 in April 15, and 214 km^2 in April 21.

The error matrix for April 18, 2010 flood map, generated using test areas, as described earlier in Section 2.2.1., is shown below in Table 4. It can be seen that the overall accuracy of the classification within the test areas was 97.2%.

Table 4. Error matrix assessing the accuracy of classification in the April 18, 2010 flood area.

		Test areas			
Generated flood map		**Open water**	**Flooded forest**	**Dry area**	**Row total**
	Open water	125	0	0	125
	Flooded forest	0	122	0	122
	Dry area	4	7	138	149
	Column total	129	129	138	396
	Open water accuracy	96.9%			
	Flooded forest accuracy	94.5%			
	Dry area accuracy	100%			
	Overall accuracy	97.2%			

3.1. Summary of results

Table 5 shows the extent of each flood, with water levels from each of the dates included. Within the borders of the Alam-Pedja Nature Reserve, the largest flood was recorded in April 18, 2010, when the flood area was 180 km^2. Also in 2011, the flood within the borders of the Alam-Pedja Nature Reserve was close to the maximum in 2010, accounting for 178 km^2 on April 21, 2011. The total flood areas in the study area showed similar trends, with the April 21, 2011 being the largest (214 km^2), followed closely by the April 18, 2010 flood of 212 km^2.

Table 5. Flood extents derived from Envisat ASAR images, and the corresponding water levels

Acquisition date	Alam-Pedja flood extent (sq. km)	Total study area flood extent (sq. km)	Water level in River Emajõgi (cm)	Water level in River Põltsamaa (cm)	Water level in River Pedja (cm)
12.01.2005	103	124	217	217	158
21.01.2005	166	188	249	64	189
08.12.2009	116	152	216	190	90
15.12.2009	129	145	221	138	19
14.04.2010	175	205	330	239	158
18.04.2010	180	212	329	222	130
24.04.2010	169	196	315	191	84
15.04.2011	156	189	295	226	176
21.04.2011	178	214	315	224	143

It can be seen in Table 5 that in most cases changes in flood areas in the Alam-Pedja Nature Reserve have a positive correlation with water level in River Emajõgi and the the total study area flood extent has a positive correlation with Pedja and Põltsamaa water levels. It can also be seen that by the time the flood area in Alam-Pedja has reached its maximum, the water level in River Põltsamaa has already dropped. This shows that the floods are caused mainly by water originating from snowmelt and precipitation around the floodplain, which flows gradually to lower-elevated areas in the Alam-Pedja Nature Reserve from higher-elevated areas around it.

4. Discussion

4.1. Uncertainties in classification

Some uncertainties in classifying the ASAR images arose due to broad spatial resolution and the lack of detailed information about conditions on the ground during the image acquisitions. Specific fieldwork campaign could have mitigated the uncertainties faced by providing ground truth data and therefore possibly increased the accuracy of the maps. Additional classification in training areas could also help in increasing the accuracy, i.e. drawing training areas on different forest and bush types and

different classes of open areas (grassland, soil, etc.). Such way the algorithm for flood detection could be improved to distinguish between different types of flooded areas. This type of precise classification, however, would require extensive field campaign to ensure its correctness.

It was noted by the author that there was a significant area around the river Emajõgi, completely surrounded by flooded areas, which was classified as non-flooded in every case. The area is shown in Figure 17. A digital elevation model (DEM) of the region, provided by the Estonian Land Board, was examined to find potential physical barriers for the flood. It was concluded that there was no justification for the area to be non-flooded, as the terrain in the region was flat and elevation lower than surrounding flooded forested regions.

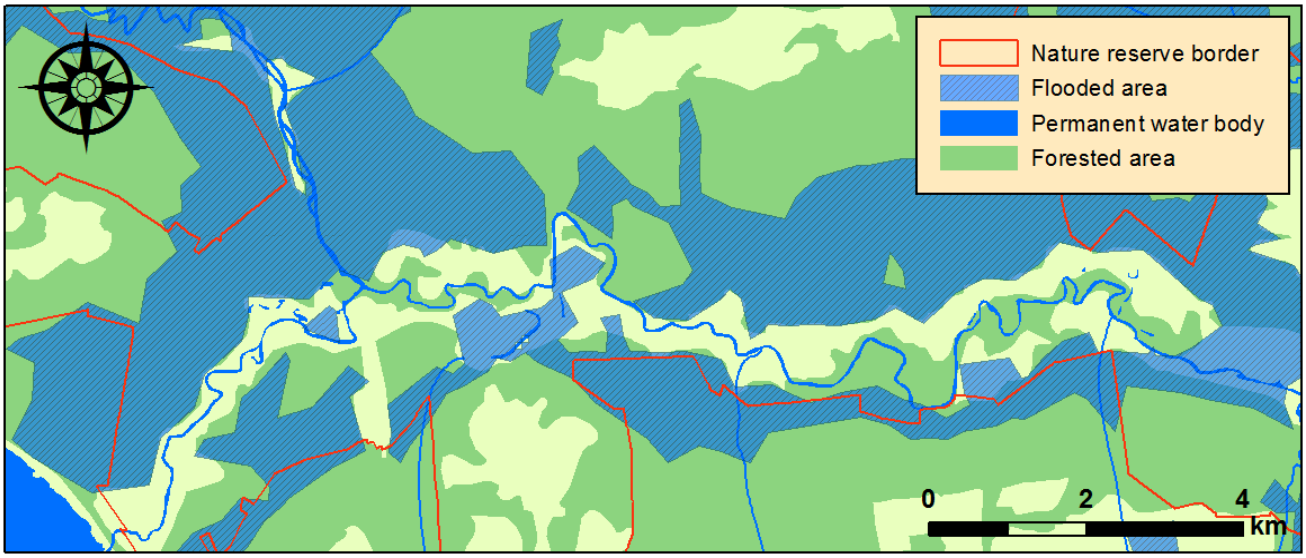

Figure 17. Outtake of the January 21, 2005 flood map, showing the potentially misclassified area around the river Emajõgi.

A very likely cause for such phenomenon is the broad spatial resolution of the Envisat ASAR images (150 m). As noted previously in Section 1.4, flooded pixels that contain both open floods (low backscatter) and shrubs or trees (very high backscatter), have their values averaged to a medium level, resulting in misclassification as non-flooded. It can also be seen in Figure 17 that there was both forested and non-forested regions present in the region. In such regions, manual DEM-based corrections could be applied to avoid misclassification due to broad spatial resolution. However, for this study, manual DEM-based corrections were out of the scope and were not applied.

4.2. Reference data

It should be noted that for improving the accuracy of flood delineation algorithms, optical images have been used in previous studies (e. g. Henry, et al., 2006). Optical images could be used to remove uncertainties, such as areas with no justification to be non-flooded classified as flooded, described in the previous section. However, there were no optical remote sensing images available around most of

the SAR image acquisitions used for this study. The only reference data available was in situ imagery, provided by Voormansik et al. (2014) for the image of April 18, 2010, and the rest of the images were scaled to have the value ranges match those of the April 18, 2010 image. In such cases the only significant difference in backscatter values in the images used should be caused by the presence of water, which was studied for flood detection, as the terrain in the region is flat and urban areas were subtracted from the images. Additional reference images could also have allowed the generation of additional test areas for accuracy assessment to enhance the representative value of the test areas. Currently the accuracy was assessed on test areas constituting 1% of the flood area.

One can argue that optical reference imagery is necessary for each SAR image to prove the validity of any SAR-based flood maps. However, SAR-based flood mapping is a developed field (Wang, et al., 1995; Townsend, 2002; Martinez & Toan, 2007; Martinis, et al., 2009) and SAR imagery is in many cases the only source of remotely sensed data for floods, as cloud cover and vegetation may cover the floodplain, making optical data inferior to SAR. In emergency situations, the rapidity of delivery is necessary, so it is important to provide possibilities for mapping floods using SAR data independently of other imagery (Martinis, et al., 2009). Using existing layers of geographical information data, such as weather and land cover data, can provide some reference and therefore can significantly improve the accuracy of SAR-based flood maps. In this study, Corine land cover data and precipitation data was used for such purposes.

4.3. The future of SAR flood detection

As the Envisat mission ended in 2012, a new satellite providing C-band SAR imagery, Sentinel-1a, was launched by ESA in April 2014. An additional satellite of the same mission, Sentinel-1b, is currently scheduled to launch in 2016 (ESA, 2014c). The new mission provides images in 4 imaging modes with spatial resolution down to 5 meters. The revisit time for Sentinel-1a, combining the ascending and descending pass, is down to 6 days, and with the launch of Sentinel-1b, it will be possible to bring the revisit time down to 3 days (ESA, 2013). The increased revisit time will highly improve the capability to rapidly map floods, and finer spatial resolution can help improve the accuracy of flood maps. Such data can also be combined by data from earlier sensors such as the Envisat ASAR, to generate flood timelines over long-term periods, and develop models for predicting potential future floods.

There is currently a trend towards the development of fully automated flood detection algorithms. In recent years, several works have been published (e.g. Martinis, et al., 2009; Martinis, 2010; Matgen, et al., 2011), discussing the state of development, opportunities and challenges of such tools. Martinis et

al. (2014) present a model for fully automated flood detection using X-band SAR, opening a new perspective for disaster monitoring. Such development makes it possible to map vast numbers of threatened areas very rapidly and provides the potential to develop near real-time flood monitoring capabilities, crucial for crisis management and other applications requiring timely information. Currently, flood mapping services are provided mostly on-demand (Martinis, et al., 2014); fully automatic procedures combined with quick revisit satellites will provide the capability to run near real-time databases, providing more timely and lower-cost services to anyone in need.

5. Conclusion

This study demonstrated the capability to map floods in the Alam-Pedja Nature Reserve in Estonia, using SAR imagery. Water level data was analysed to detect the potential floods in the focus period of 2005-2011, and a total of 24 Envisat ASAR C-band HH-polarized SAR images with spatial resolution of 150 m were acquired for the study, out of which nine images proved suitable. The results of the study were nine SAR-based flood maps of the Alam-Pedja Nature Reserve from January 2005, December 2009, April 2010 and April 2011.

These images were first processed in Next ESA SAR Toolbox. A despeckling procedure was held to remove the speckle noise in the images. On the image of April 18, 2010, training areas of flooded open areas, non-flooded areas, and flooded forested areas were created, using geo-referenced photos taken for a previous study by Voormansik et al. (2014) as reference data. The rest of the images were calibrated to match the values of the April 18, 2010 ASAR image, to remove differences in backscatter values caused by differences in incidence angle. A split-based manual thresholding algorithm was then used on each image, creating Boolean images of flooded and non-flooded regions. The resulting Boolean images were transferred to ESRI ArcMap software, where the images were vectorized, and composed into flood maps. The flood extents were then calculated both within the Alam-Pedja Nature Reserve and in an additional 1951 km^2 study area around it. Test areas were selected on the ASAR image of April 18, 2010, constituting 1% of the total flood area. An error matrix was generated to assess the accuracy of the classification.

The results showed that the largest floods within the Alam-Pedja Nature Reserve occurred in April 18, 2010 and April 21, 2011, when the flood areas were sized 180 km^2 and 178 km^2, respectively. In the surrounding study area, the largest areas considered as flooded were recorded in the same dates, with floods extending to 212 and 214 km^2, respectively. According to the error matrix generated from the test areas, the overall accuracy of the classification was 97.2%.

It could be seen that in most cases changes in flood areas in the Alam-Pedja Nature Reserve had a positive correlation with water level in River Emajõgi and the total study area flood extent was in positive correlation with Pedja and Põltsamaa water levels. It could also be seen that by the time the flood area in Alam-Pedja had reached its maximum, the water level in River Põltsamaa has already dropped. This shows that floods were caused mainly by water originating from snowmelt and precipitation around the floodplain, which flowed gradually to lower-elevated areas in the Alam-Pedja Nature Reserve from higher-elevated areas around it.

The broad resolution of Envisat ASAR images caused some errors in classification. The presence of shrubs or trees in the same pixels with open flooded areas, had their values averaged to a medium level, resulting in misclassification as non-flooded areas, although there was no justification of the regions to be non-flooded, as they were surrounded by higher elevated areas being flooded. Such errors can be mitigated by DEM-based corrections in future works.

Specific fieldworks on each acquisition period would have helped to decrease uncertainties and increase the accuracy of the flood maps. However, as the used SAR imagery was obtained from archives, specific fieldworks were not conducted.

With the new capabilities of the ESA Sentinel-1 mission, C-band SAR-based flood mapping can be improved a lot in the near future. The new mission provides improved spatial and temporal resolution, resulting in higher accuracy flood maps and providing the possibility to map the temporal dynamics of each flood more accurately.

Currently, the development of fully automated flood monitoring algorithms for X- and C-band SAR is in progress. Such development makes it possible to map vast numbers of inundated areas very rapidly and provides the potential to develop near real-time flood monitoring services, crucial for crisis management and other applications requiring timely information.

Üleujutuste kaardistamine tehisava-radari mõõtmiste baasil Alam-Pedja looduskaitsealal 2005-2011 aastatel

Martin Jüssi

Kokkuvõte

Käesoleva magistritöö eesmärgiks oli kaardistada üleujutusi Alam-Pedja looduskaitsealal 2005-2011 aastatel tehisava-radari (*i k synthetic aperture radar - SAR*) mõõtmiste baasil. Töö esimene peatükk tutvustab üleujutuste kaardistamise vajalikkust ning radarkaugseire sobivust selleks tööks. Teises peatükis kirjeldatakse antud magistritöös kasutatavaid andmeid ja metoodikat. Kolmandas peatükis esitatakse saadud tulemused ning neljandas peatükis tulemuste arutelu koos uurimisteema tulevikuvõimaluste tutvustamisega. Viiendas peatükis esitatakse töö kokkuvõte.

Töö teostamiseks analüüsiti uurimisperioodi veetasemeandmeid Eesti Ilmateenistuse Tõrve, Pajusi ja Tartu-Kvissentali mõõtmisjaamadest ning telliti huvipakkuvatest perioodidest tehisava-radari pildid. Kasutatud pildid pärinesid Euroopa Kosmoseagentuuri satelliidi Envisat sensorilt ASAR (*advanced synthetic aperture radar*). Huvipakkuvast perioodist oli üleujutuste tuvastamiseks sobilikke pilte üheksa. Envisat ASARi andmed olid mõõdetud HH-polarisatsiooniga C-kanalis 5.6 cm lainepikkusel ning 150-meetrise ruumilise lahutusega. Töö tulemuseks oli üheksa üleujutuskaarti, neljast perioodist 2005. aasta jaanuaris, 2009. aasta detsembris ning 2010. ja 2011. aasta aprillis.

Tellitud radaripilte töödeldi esmalt rasterkujul Next ESA SAR Toolbox tarkvaras. 2010. aasta 18. aprillist pärit pildilt, mis oli varasematel välitöödel tehtud fotodega dokumenteeritud, tuvastati treeningalad kuiva, üleujutatud lageda ala ning üleujutatud metsa jaoks. Saadud väärtuste võrdlemisel tuvastati piirväärtused kuivade ning veega üleujutatud pikslite vahel ning koostati Boole'i kaardid. Klassifitseerimistäpsust kontrolliti testalade abil, mis moodustasid kogu üleujutusest 1%. Ülejäänud uurimistöös kasutatud Envisat ASARi pildid viidi lineaarse skaleerimise abil dokumenteeritud fotoga samale skaalale, et välistada pildistamisnurgast tulenevaid erinevusi pikslite heleduses ning koostati samuti Boole'i kaardid.

Saadud Boole'i kaardid vektoriseeriti ESRI ArcMap tarkvaras ning koostati üleujutuskaardid. Üleujutuste ulatus arvutati Alam-Pedja looduskaitseala piires. Esitati ka tulemused laiemast 1951 km^2 suurusest alast Alam-Pedja looduskaitseala ümber, kuid neid tulemusi ei saanud referentsandmete puudumise tõttu kinnitada. Tulemustest selgus, et suurimad üleujutused Alam-Pedja looduskaitsealal olid 2010. aasta 24. aprillil, kui üleujutatud oli 214 km^2 suurune ala ning 2011. aasta 15. aprillil, kui üleujutuse suurus oli 203 km^2. Testaladel kirjeldatud kaardistamise täpsuseks oli 97.2%.

2009. aasta detsembris ja 2010. aasta aprillis erines üleujutuste dünaamika Alam-Pedja looduskaitsealal samal ajal ümbritsevatel aladel toimunud üleujutuste dünaamikast. 8. ja 15. detsembri vahel kasvas üleujutusala looduskaitseala piires 116-st 129 km^2-ni, vähenedes samal ajal kogu uurimisala piires 152-lt 145 km^2-ni. Sellist muutust põhjendati vee kokkuvoolamisega Alam-Pedja looduskaitseala ümbritsevatelt aladelt madalamale.

Probleemina ilmnes ASAR-piltide jäme ruumiline lahutus. Madalat radarisignaali tagasihajumist tootvate tasaste üleujutatud aladega samadesse pikslitesse langevad puud ja põõsad, mis toodavad veega koosmõjus väga kõrget signaali tagasihajumist, jäid keskmistamise tõttu „märjaks“ klassifitseeritud pikslite hulgast välja. Selliseid vigu saaks vähendada manuaalse kõrgusmudelil põhineva paranduse abil, mida selle töö mahus ei tehtud.

Kaartide täpsust oleks aidanud suurendada välitööde tegemine kõigil uuritavatel perioodidel. Kuna töös kasutati arhiiviandmeid, siis spetsiaalseid välitöid ei tehtud ning kasutati saadaval olevaid varem tehtud välitööde andmed 2010. aasta 18. aprilli üleujutusest.

Seoses Euroopa Kosmoseagentuuri uue Sentinel-1 missiooni algusega paranevad lähitulevikus C-kanali SAR-il põhinevad üleujutuste tuvastamise võimalused oluliselt. Missioon võimaldab saada täpsema ruumilise ja ajalise lahutusega radarimõõtmisi, võimaldades kaardistada üleujutuste dünaamikat kuni 3-päevaste vahedega ning kuni 30-meetrise ruumilise lahutusega. Samuti on praegu käimas täisautomaatsete SAR-il põhinevate üleujutuste tuvastamise algoritmide väljatöötamine. Uute ja paremate instrumentide ning uudse metoodika abil on tulevikus võimalik üleujutusi kaardistada oluliselt kiiremini ja efektiivsemalt kui seniste manuaalsete protseduuride abil.

Acknowledgments

My sincere gratitude goes to my supervisors Kaupo Voormansik, Kārlis Zālīte and Tanel Tamm, for their dedicated time for directing and supporting the progress of this thesis. I would also like to thank the European Space Agency for providing the Envisat ASAR images for this study, Regio Ltd. for vector data, Estonian Land Board for the digital elevation model, and the Estonian Weather Service for water level and weather data.

Martin Jüssi

References

Aaviksoo, K., Paal, J. & Dišlis, T., 2000. Mapping of wetland habitat diversity using satellite data and GIS: An example from the Alam-Pedja Nature Reserve, Estonia. *Proceedings of the Estonian Academy of Sciences, Biology and Ecology.*

Baghdadi, N., Bernier, M., Gauthier, R. & Neeson, I., 2001. Evaluation of C-band SAR data for wetlands mapping. *International Journal of Remote Sensing,* 22(1), pp. 71-88.

Bates, B. D. & De Roo, A. P. J., 2000. A simple raster-based model for flood inundation simulation. *Journal of Hydrology,* Volume 236, pp. 54-77.

Canada Centre for Remote Sensing, 2015. *Fundamentals of Remote Sensing.* [Online] Available at: http://www.nrcan.gc.ca/sites/www.nrcan.gc.ca/files/earthsciences/pdf/resource/tutor/fundam/pdf/fundamentals_e.pdf [Accessed 3 March 2015].

Centre for Remote Imaging, Sensing & Processing, 2001. *SAR Imaging - Frequency, Polarisation and Incident Angle.* [Online] Available at: http://www.crisp.nus.edu.sg/~research/tutorial/freqpol.htm [Accessed 2 January 2015].

Congalton, R. G., 1991. A review of assessing the accuracy of classifications of remotely sensed data. *Remote sensing of environment,* 37(1), pp. 35-46.

Drake, B. & Shuchman, R. A., 1974. *Feasibility of using multiplexed SLAR imagery for water resources management and mapping vegetation communities.* Ann Arbor, MI, USA, Environmental Research Institute of Michigan, p. 714–724.

Enslin, W. R. & Sullivan, M. C., 1974. *The use of color infrared photography for wetlands assessment,* Detroit: Michigan State University.

ESA, 2013. *Sentinel-1 user handbook.* [Online] Available at: https://earth.esa.int/documents/247904/685163/Sentinel-1_User_Handbook [Accessed 2 January 2015].

ESA, 2014a. *What is Envisat?.* [Online] Available at: https://earth.esa.int/web/guest/missions/esa-operational-eo-missions/envisat [Accessed 26 December 2014].

ESA, 2014b. *NEST - next ESA SAR toolbox.* [Online] Available at: https://earth.esa.int/web/nest/home [Accessed 27 December 2014].

ESA, 2014c. *Sentinel-1 Mission Details.* [Online] Available at: https://earth.esa.int/web/guest/missions/esa-operational-eo-missions/sentinel-1 [Accessed 2 January 2015].

Estonian Ministry of Environment, 2007. *Estonia has 15 significant flood risk regions.* [Online] Available at: http://www.envir.ee/392870 [Accessed 15 June 2014].

Estonian Ministry of Environment, 2013. *Üleujutusohuga seotud riskide esialgse hinnangu aruanne.* [Online] Available at: http://www.envir.ee/sites/default/files/yleujutusohugaseotudriskidearuanne.pdf [Accessed 15 June 2014].

European Environment Agency, 2006. *Corine Land Cover 2006 raster data.* [Online] Available at: http://www.eea.europa.eu/data-and-maps/data/corine-land-cover-2006-raster-2 [Accessed 29 December 2014].

EWS, 2014. *Observation data.* [Online] Available at: http://www.ilmateenistus.ee/ilm/ilmavaatlused/vaatlusandmed/kaart/?lang=en [Accessed 28 December 2014].

Griffis, T. J., Rouse, W. R. & Waddington, J. M., 2000. Interannual variability of net ecosystem CO2 exchange at a subarctic fen. *Global Biogeochemical Cycles,* 14(4), pp. 1109-1121.

Henry, J.-B., Chastanet, B., Fellah, K. & Desnos, Y.-L., 2006. Envisat multi-polarized ASAR data for flood mapping. *International Journal of Remote Sensing,* 27(10), pp. 1921-1929.

Hess, L. L., Melack, J. M. & Simonett, D. S., 1990. Radar detection of flooding beneath the forest canopy: a review. *International Journal of Remote Sensing,* 11(7), p. 1313–1325.

Horritt, M. et al., 2003. Waterline mapping in flooded vegetation from airborne SAR imagery. *Remote Sensing of Environment,* 85(3), p. 271–281.

Johnston, R. M. & Barson, M. M., 1990. Use of multitemporal Landsat Thematic Mapper imagery for mapping and monitoring of wetlands. *Fiftieth Australasian Remote Sensing Conference,* p. 1125–1128.

Jongman, B. et al., 2014. Increasing stress on disaster-risk finance due to large floods. *Nature Climate Change,* Volume 4, pp. 264-268.

Kasische, E. S. & Bourgeau-Chavez, L. L., 1997. Monitoring South Florida wetlands using ERS-1 SAR imagery. *hotogrammetric Engineering & Remote Sensing,* 63(3), pp. 281-291.

Kasische, E. S., Melaneck, J. M. & Dobson, M. C., 1997. The use of imaging radars for ecological applications – A review. *Remote Sensing of Environment,* 59(2), pp. 141-156.

Kogan, F., Powell, A. M. & Fedorov, O., 2011. *Flood Monitoring from SAR Data,* Heidelberg, Germany: Springer.

Koskinen, J. T., Pulliainen, J. T. & Hallikainen, M. T., 1997. The use of ERS-1 SAR data in snow melt monitoring. *IEEE Transactions on Geoscience and Remote Sensing,* 35(3), pp. 601-610.

Kuenzer, C. et al., 2013. Flood Mapping and Flood Dynamics of the Mekong Delta: ENVISAT ASAR WSM Based Time Series Analyses. *Remote Sensing,* Volume 5, pp. 687-715.

Kuplich, T. M., Freitas, C. C. & Soares, J. V., 2000. The study of ERS-1 SAR and Landsat TM synergism for land use classification. *International Journal of Remote Sensing,* 21(10), pp. 2101-2111.

Lee, J. S. et al., 1994. Speckle filtering of Synthetic Aperture Radar images: a review. *Remote Sensing Reviews,* Volume 8, pp. 313-340.

Lowry, R. T., Langham, E. J. & Mudry, N., 1981. Preliminary analysis of SAR mapping of the Manitoba flood, May 1979. *Proceedings series-American Water Resources Association.*

Martinez, J.-M. & Toan, T., 2007. Mapping of flood dynamics and spatial distribution of vegetation in the Amazon floodplain using multitemporal SAR data. *Remote Sensing of Environment,* Volume 108, pp. 209-223.

Martinis, S., 2010. Automatic near real-time flood detection in high resolution X-band synthetic aperture radar satellite data using context-based classification on irregular graphs. *Dissertation der Fakultät für Geowissenschaften der Ludwig-Maximilians-Universität München.*

Martinis, S., Kersten, J. & Twele, A., 2014. A fully automated TerraSAR-X based flood service. *ISPRS Journal of Photogrammetry and Remote Sensing.*

Martinis, S., Twele, A. & Voigt, S., 2009. Towards operational near real-time flood detection using a split-based automatic thresholding procedure on high resolution TerraSAR-X data. *Natural Hazards and Earth System Sciences,* Volume 9, p. 303–314.

Mascarenhas, N. D. A., 1997. An Overview of Speckle Noise Filtering in SAR Images. *Image Processing Techniques, First Latino-American Seminar on Radar Remote Sensing,* p. 71.

Mason, D. C. et al., 2010. Flood detection in urban areas using TerraSAR-X. *IEEE Transactions on Geoscience and Remote Sensing,* 48(2), pp. 882-894.

Matgen, P. et al., 2011. Towards an automated SAR-based flood monitoring system: Lessons learned from two case studies. *Physics and Chemistry of the Earth, Parts A/B/C,* 36(7), pp. 241-252.

Nardi, F. et al., 2013. Comparing a large-scale DEM-based floodplain delineation algorithm with standard flood maps: the tiber river case study. *Irrigation and Drainage,* 62(2), pp. 11-19.

Sarti, F., Inglada, J., R., L. & Pultz, T., 2001. *Risk management using remote sensing data: moving from scientific to operational applications.* Foz do Iguaçu, Brasil, s.n.

Schumann, G. et al., 2007. High-resolution 3-D flood information from radar imagery for flood hazard management. *IEEE Transactions on Geoscience and Remote Sensing,* 45(6), p. 1715–1725.

Smith, D. I., 1994. Flood damage estimation- A review of urban stage-damage curves and loss functions. *Water S. A.,* 20(3), pp. 231-238.

Smith, L. C., 1997. Satelite Remote Sensing of River Inundation Area, Stage, and Discharge: A Review. *Hydrological Processes,* Volume 11, pp. 1427-1439.

Townsend, P. A., 2002. Relationships between forest structure and the detection of flood inundation in forested wetlands using C-band SAR. *International Journal of Remote Sensing,* 23(3), pp. 443-460.

Van der Sande, C. J., De Jong, S. M. & De Roo, A. P. J., 2003. A segmentation and classification approach of IKONOS-2 imagery for land cover mapping to assist flood risk and flood damage assessment. *International Journal of Applied Earth Observation and Geoinformation,* 4(3), p. 217–229.

Voormansik, K. et al., 2014. Flood Mapping With TerraSAR-X in Forested Regions in Estonia. *IEEE Journal of Selected Topics in Applied Earth Observations and Remote Sensing,* 7(2).

Wang, Y., Hess, L. L., Filoso, S. & Melack, J. M., 1995. Understanding the radar backscattering from flooded and non-flooded Amazonian forests: Results from canopy backscatter modeling. *Remote Sensing of Environment,* Volume 54, pp. 324-332.

Zalite, K. et al., 2013. Effects of inundated vegetation on X-Band HH–VV backscatter and phase difference. *IEEE Journal of Selected Topics in Applied Earth Observations and Remote Sensing,* 7(4), pp. 1402-1406.

Annexes

In this section, pre-processed Envisat ASAR images, used in this study, are presented. White areas correspond to flooded forest and black areas to open water, grey areas are typically non-flooded.

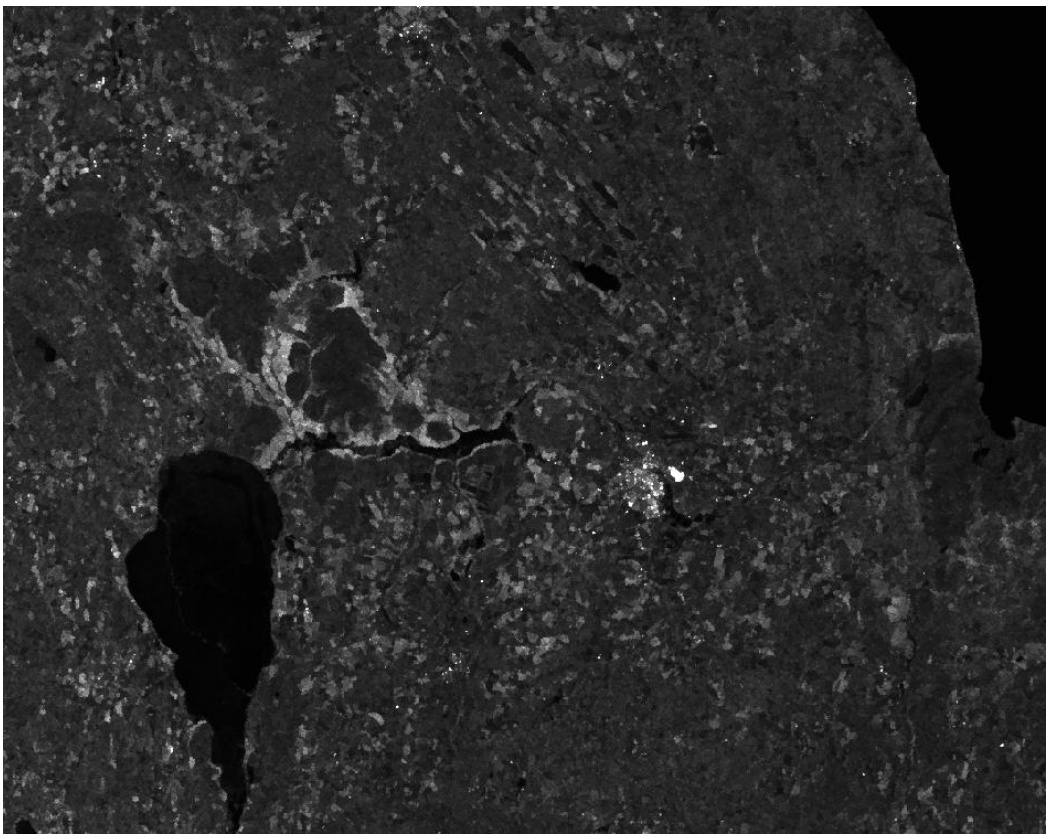

Annex 1. ASAR image of January 12, 2005

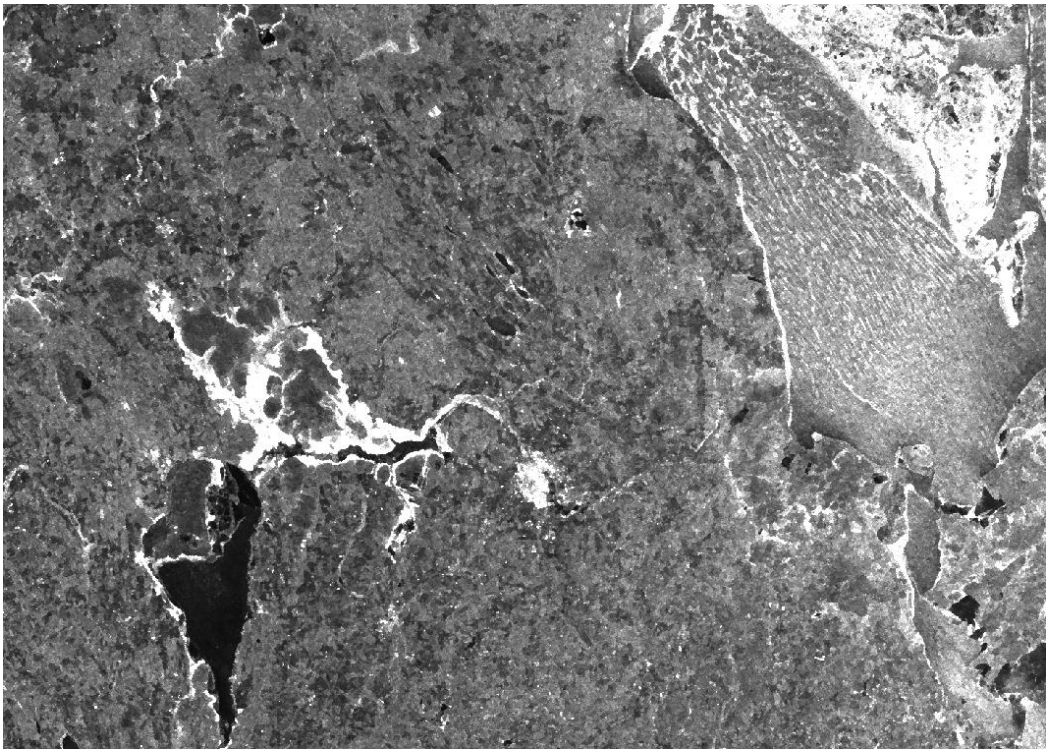

Annex 2. ASAR image of January 21, 2005

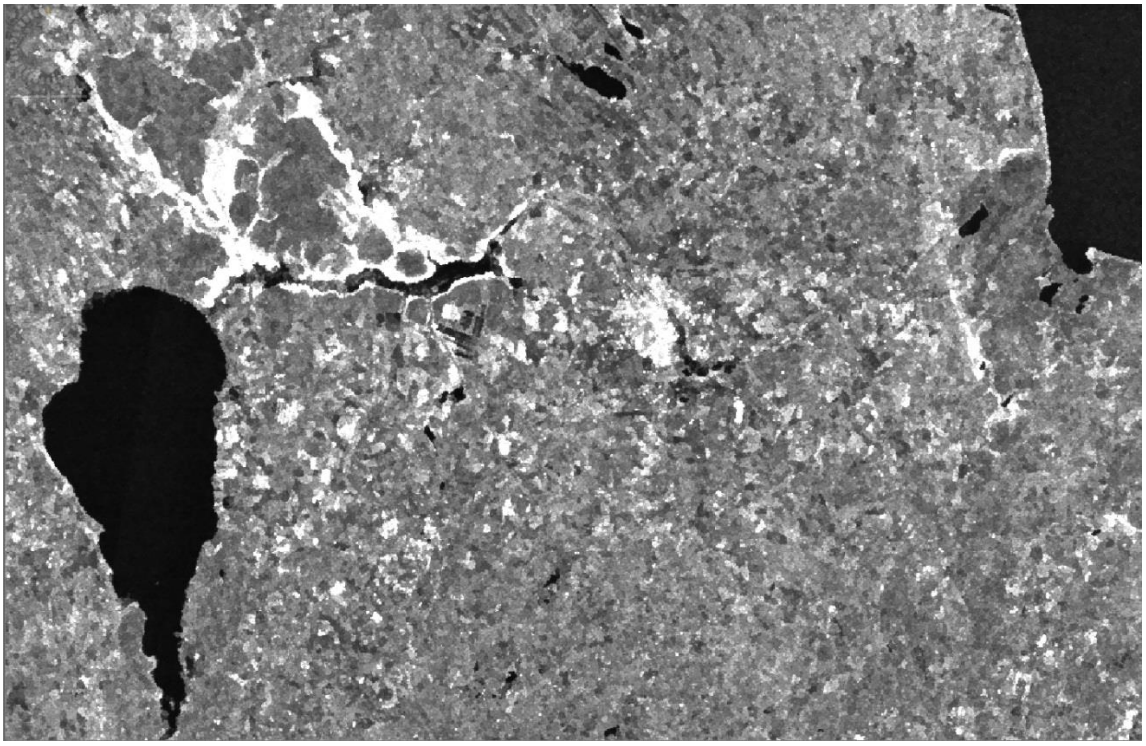

Annex 3. ASAR image of December 8, 2009

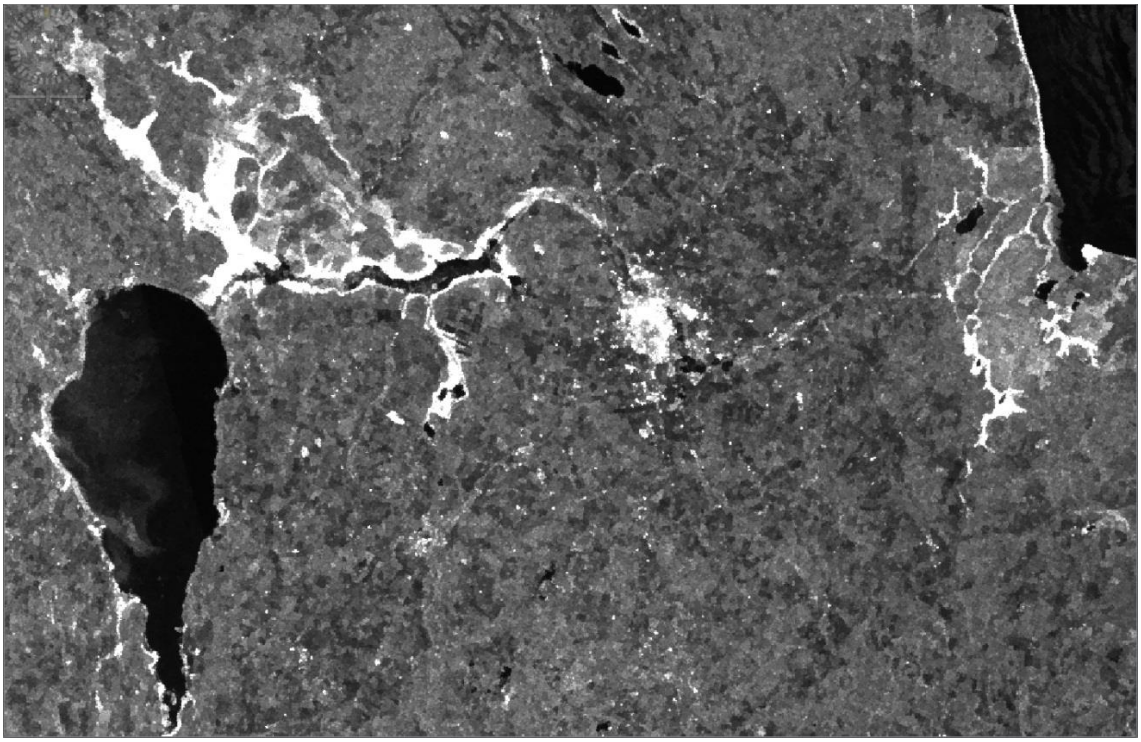

Annex 4. ASAR image of December 15, 2009

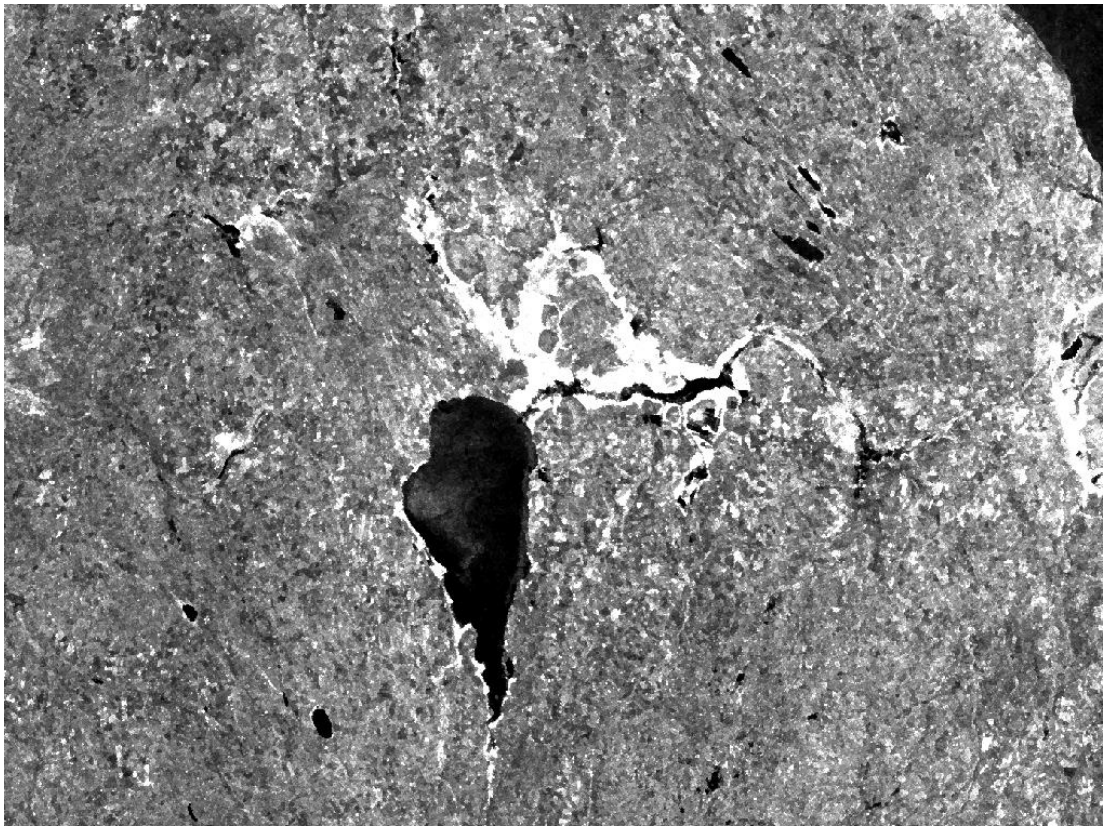

Annex 5. ASAR image of April 14, 2010

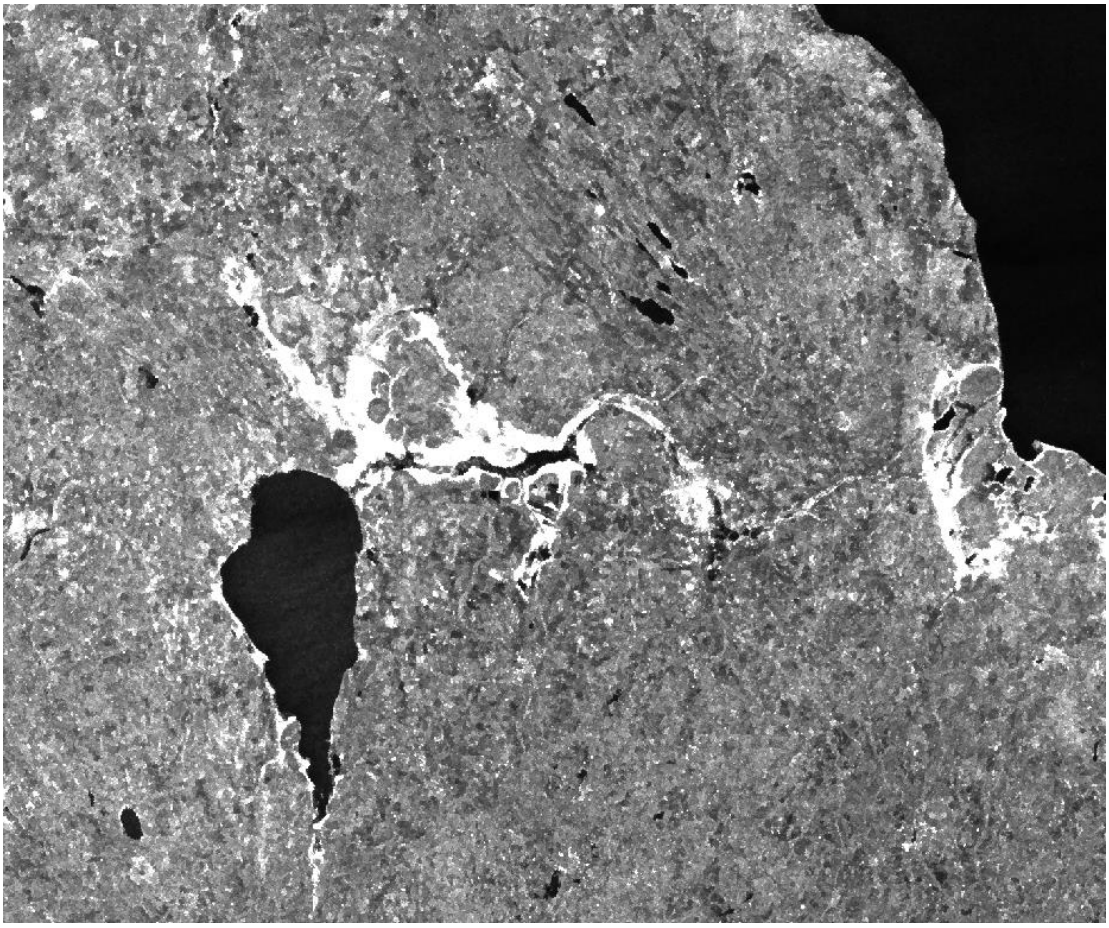

Annex 6. ASAR image of April 18, 2010

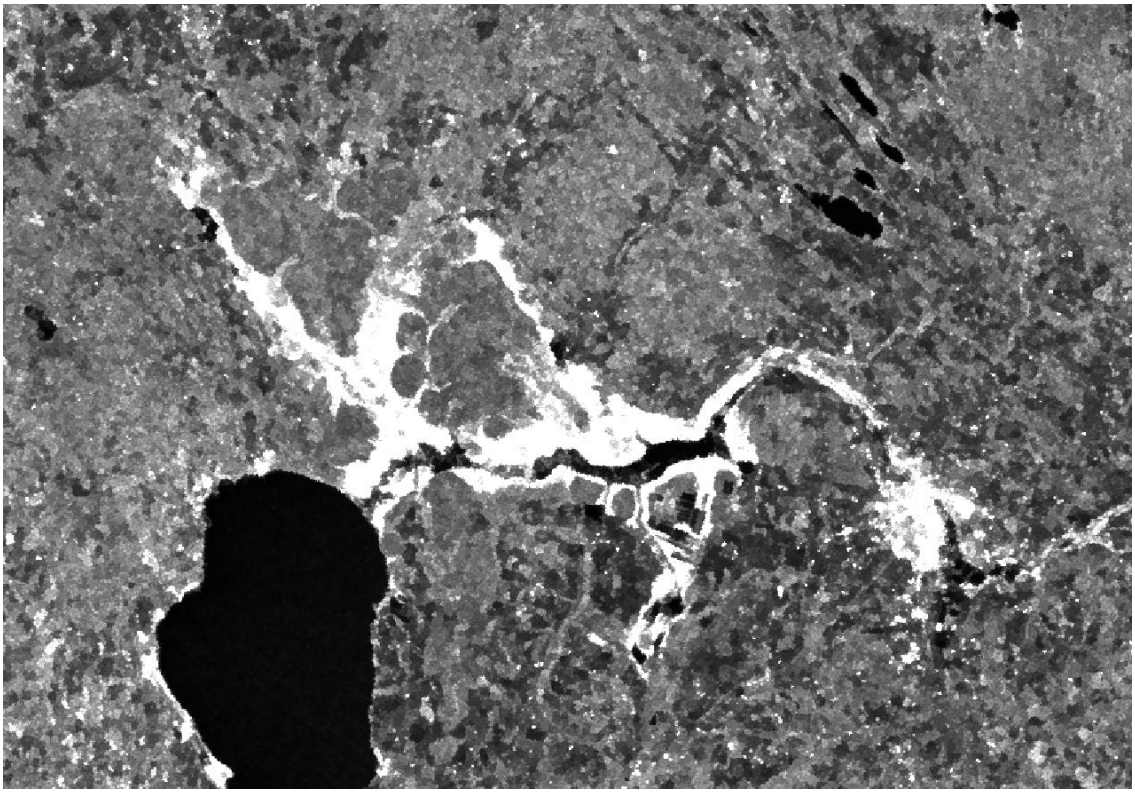

Annex 7. ASAR image of April 24, 2010

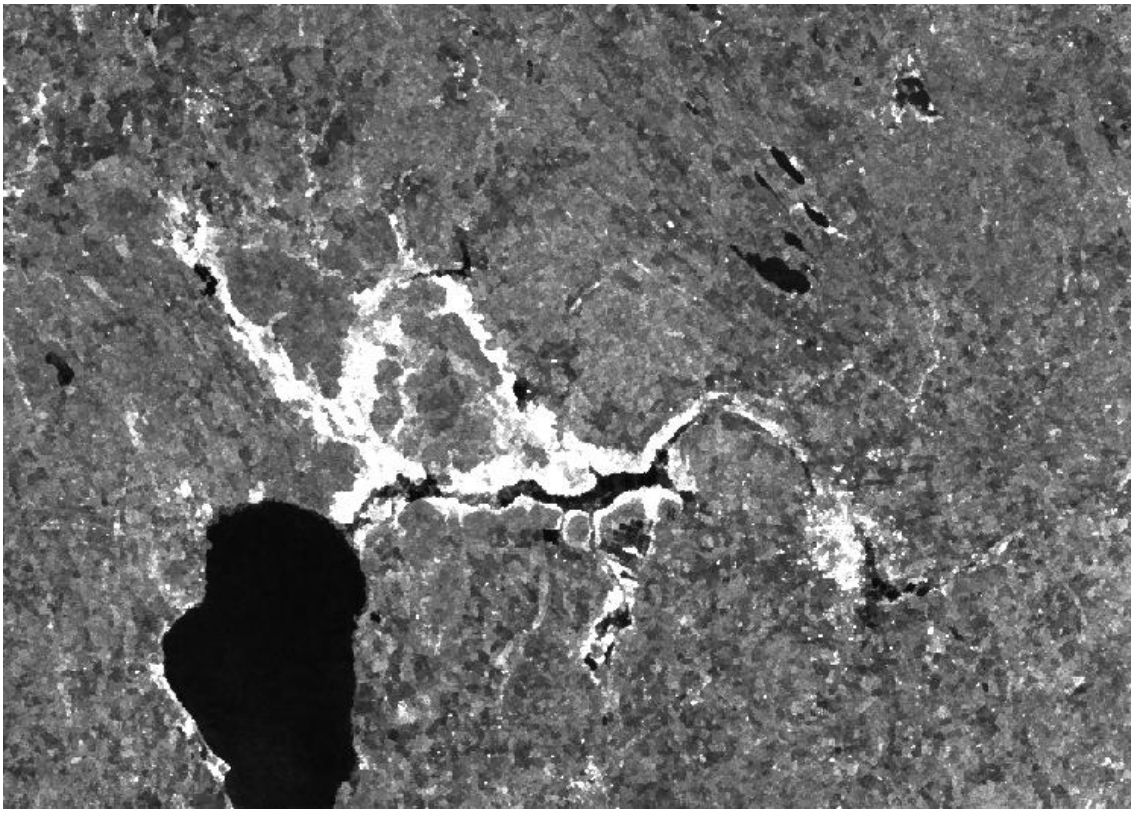

Annex 8. ASAR image of April 15, 2011

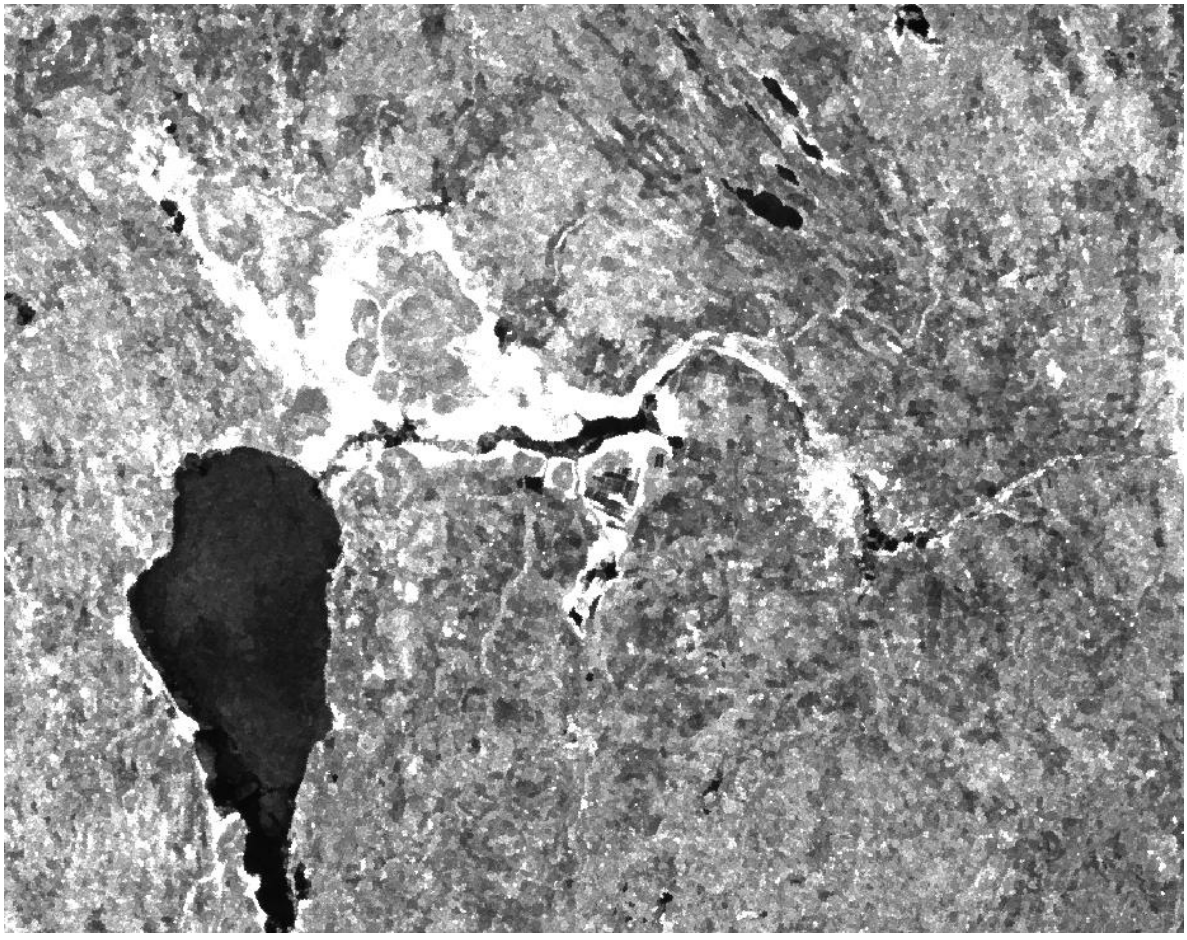

Annex 9. ASAR image of April 21, 2011

Lihtlitsents lõputöö reprodutseerimiseks ja lõputöö üldsusele kättesaadavaks tegemiseks

Mina, Martin Jüssi,

1. annan Tartu Ülikoolile tasuta loa (lihtlitsentsi) enda loodud teose *Synthetic Aperture Radar based flood mapping in the Alam-Pedja Nature Reserve in years 2005-2011*, mille juhendajad on Kaupo Voormansik, Kārlis Zālīte, Tanel Tamm,

1.1. reprodutseerimiseks säilitamise ja üldsusele kättesaadavaks tegemise eesmärgil, sealhulgas digitaalarhiivi DSpace-is lisamise eesmärgil kuni autoriõiguse kehtivuse tähtaja lõppemiseni;

1.2. üldsusele kättesaadavaks tegemiseks Tartu Ülikooli veebikeskkonna kaudu, sealhulgas digitaalarhiivi DSpace´i kaudu kuni autoriõiguse kehtivuse tähtaja lõppemiseni.

2. olen teadlik, et punktis 1 nimetatud õigused jäävad alles ka autorile.

3. kinnitan, et lihtlitsentsi andmisega ei rikuta teiste isikute intellektuaalomandi ega isikuandmete kaitse seadusest tulenevaid õigusi.

Tartus, 09.05.2015